Available online at www.sciencedirect.com
ScienceDirect
Journal of Sound and Vibration 320 (2009) 289–321
JOURNAL OF SOUND AND VIBRATION
www.elsevier.com/locate/jsvi

Sound propagation in narrow tubes including effects of viscothermal and turbulent damping with application to charge air coolers

Magnus Knutsson[a,b,*], Mats Åbom[b]

[a]*Volvo Car Corporation, SE-405 31 Göteborg, Sweden*
[b]*KTH CICERO, The Marcus Wallenberg Laboratory, Royal Institute of Technology, SE-100 44 Stockholm, Sweden*

Received 23 November 2007; received in revised form 3 June 2008; accepted 15 July 2008
Handling Editor: C.L. Morfey
Available online 27 August 2008

Abstract

Charge air coolers (CACs) are used on turbocharged internal combustion engines to enhance the overall gas-exchange performance. The cooling of the charged air results in higher density and thus volumetric efficiency. It is also important for petrol engines that the knock margin increases with reduced charge air temperature. A property that is still not very well investigated is the sound transmission through a CAC. The losses, due to viscous and thermal boundary layers as well as turbulence, in the narrow cooling tubes result in frequency dependent attenuation of the transmitted sound that is significant and dependent on the flow conditions. Normally, the cross-sections of the cooling tubes are neither circular nor rectangular, which is why no analytical solution accounting for a superimposed mean flow exists. The cross-dimensions of the connecting tanks, located on each side of the cooling tubes, are large compared to the diameters of the inlet and outlet ducts. Three-dimensional effects will therefore be important at frequencies significantly lower than the cut-on frequencies of the inlet/outlet ducts. In this study the two-dimensional finite element solution scheme for sound propagation in narrow tubes, including the effect of viscous and thermal boundary layers, originally derived by Astley and Cummings [Wave propagation in catalytic converters: Formulation of the problem and finite element scheme, *Journal of Sound and Vibration* 188 (5) (1995) 635–657] is used to extract two-ports to represent the cooling tubes. The approximate solutions for sound propagation, accounting for viscothermal and turbulent boundary layers derived by Dokumaci [Sound transmission in narrow pipes with superimposed uniform mean flow and acoustic modelling of automobile catalytic converters, *Journal of Sound and Vibration* 182 (5) (1995) 799–808] and Howe [The damping of sound by wall turbulent shear layers, *Journal of the Acoustical Society of America* 98 (3) (1995) 1723–1730], are additionally calculated for corresponding circular cross-sections for comparison and discussion. The two-ports are thereafter combined with numerically obtained multi-ports, representing the connecting tanks, in order to obtain the transmission properties for the charged air when passing the complete CAC. An attractive formalism for representation of the multi-ports based on the admittance relationship between the ports is presented. From this the first linear frequency domain model for CACs, which includes a complete treatment of losses in the cooling tubes and 3D effects in the connecting tanks is extracted in the form of a two-port. The frequency dependent transmission loss is calculated and compared to the corresponding experimental data with good agreement.

*Corresponding author at: The Marcus Wallenberg Laboratory for Sound and Vibration Research, Department of Aeronautical and Vehicle Engineering, KTH, SE-100 44 Stockholm, Sweden. Tel.: +46 73 770 9972 or +46 31 325 4064; fax: +46 8 790 61 22.
E-mail addresses: magnuskn@kth.se, mknutsso@volvocars.com (M. Knutsson).

0022-460X/$ - see front matter © 2008 Elsevier Ltd. All rights reserved.
doi:10.1016/j.jsv.2008.07.006

1. Introduction

1.1. General

The recent trend of downsizing internal combustion (IC) engines, in order to reduce fuel consumption, while using turbochargers to maintain the engine torque and power imposes additional noise phenomena not created by naturally aspirated engines. Examples of such noise sources are the whining due to unbalance in the turbo-axle and the different aerodynamic phenomena due to the high speed revolution of the turbine and compressor wheels. For the in-duct noise the aerodynamic turbo sources are normally the most important [1] producing high frequency noise [1,2] in the kHz range. In contrast the engine breathing represents low frequency noise well below 1 kHz.

Many turbocharged engines are equipped with charge air coolers (CAC), a device used to increase the overall performance of the engine. The cooling of the charged air results in higher density and thus volumetric efficiency. It is also important for petrol engines that the knock margin increases with reduced temperature. The parameters of main interest when designing a CAC are normally the pressure drop and the heat exchange efficiency. However, what seem to have been overseen are the acoustic properties, which are still not very well investigated. To the authors' knowledge the sound attenuation properties are only dealt with in two previous publications [3,4]. The models in both these references make use of two-ports (or four-poles) to assemble a complete model for a CAC. However, neither of them includes a complete treatment of the losses in the cooling tubes. According to the literature survey in Ref. [3], there are predictive models available describing the thermal efficiency [5], and also models treating flow unsteadiness [6–8] in CACs. Still they are only evaluated in terms of heat transfer performance, pressure drop and gas-exchange properties mainly affecting lower frequencies. In Refs. [9,10], Knutsson and Åbom have presented some initial parts of the work presented in this paper, which aims to make a complete model of the sound attenuating properties of CACs when there is a mean flow present.

Most CACs consist of two of the most widely used sound attenuation measures: the reactive expansion chamber, denoted in Fig. 1 by inlet/outlet tank, and the dissipative narrow cooling tubes. The assembled component thereby offers possibly underestimated capabilities for broadband noise silencing that could be used for noise optimization. As the CAC is installed downstream of the compressor (see Fig. 2), the noise that is radiated from the compressor and travels upstream towards the intake orifice is of course not affected by the CAC. However, the CAC will attenuate the compressor noise that is transmitted downstream towards the engine and will thereby reduce the amount of break-out noise that radiates through the walls of the ducts situated downstream of the CAC. It is also interesting that the low frequency engine breathing noise resulting from the motion of the intake valves as well as the overhearing of exhaust noise through the EGR-system will be reduced by the CAC. In order to take full advantage of this possibility, theoretical CAC models are required to enable optimization.

In this paper a complete CAC linear frequency domain hybrid-model based on coupling multi-ports, representing the inlet/outlet tanks, to resistive two-ports, representing the cooling tubes, is presented. The model is validated for an air-to-air charge air cooler used in passenger cars (see Fig. 3). The cooling tubes in this CAC are equipped with turbulators, as shown in Fig. 4, a folded metal sheet with large area, used to improve the heat exchange efficiency of the cooling tubes. This installation creates narrow, almost triangularly shaped (or isosceles trapezium), internal axial channels with dimensions equivalent to a hydraulic diameter

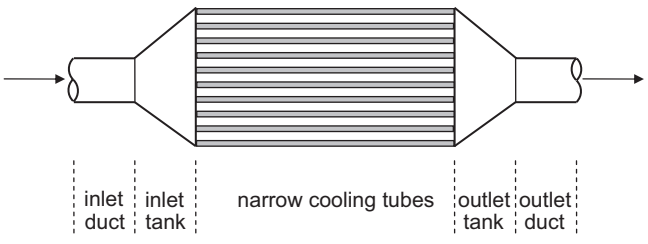

Fig. 1. Schematic representation of a generic air-to-air charge air cooler.

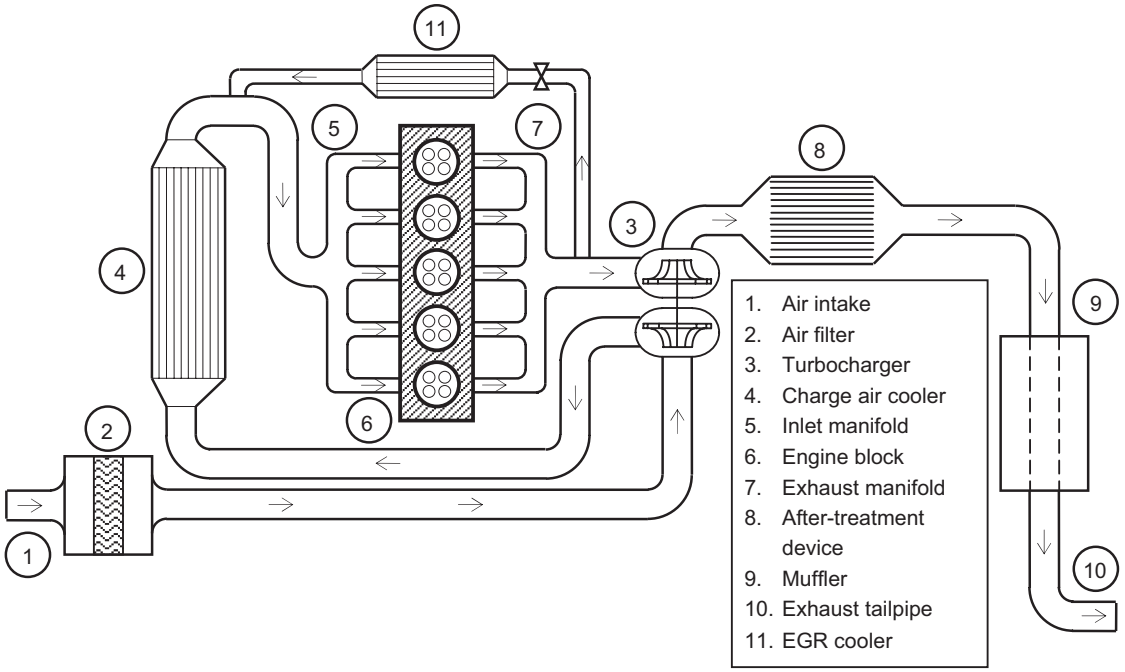

Fig. 2. Schematic representation of a turbocharged diesel engine with charge air cooler.

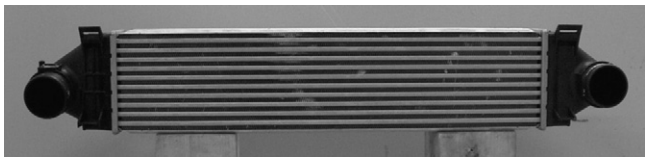

Fig. 3. Photograph of charge air cooler used for validation.

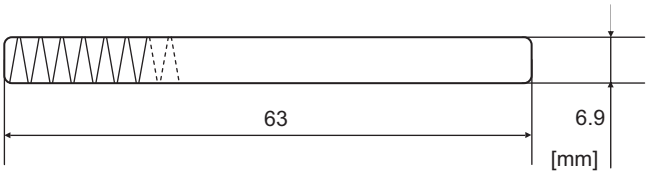

Fig. 4. Internal geometry of one single cooling tube (geometry of turbulators indicated) in validation CAC.

between 2.5 and 3 mm. The propagation of sound in such tiny ducts was found by Kirchhoff [11] to be dissipative due to viscous and thermal effects at the pipe walls. In this work he obtained the solution to the problem, without any flow present, as a complicated, complex transcendental equation which has so far not been solved analytically. In the work by Zwikker and Kosten [12] an approximate solution to the problem was found from a set of simplified equations. When flow is present the situation is somewhat more complicated and no complete theory exists. Several authors [13–22] have, however, derived solutions based on simplified equations or numerical calculations. In the present paper the solution for circular ducts by Dokumaci [14], a modified version of the numerical solution scheme for arbitrary cross-sections derived by Astley and Cummings [16] and the solution accounting for turbulence in circular ducts by Howe [26] are used to model the cooling tubes in order to determine which is the most accurate. Two-ports representing a cooling tube are extracted from the three solutions, which has not to the authors' knowledge previously been done for the latter

two. The effect of approximating cross-sections that are shaped as isosceles trapeziums with circular geometries, where the hydraulic diameter is equivalent, is studied for cases where laminar or turbulent flow is present.

As the cross-dimensions of the connecting tanks are the largest in the charged air system they will define the upper frequency limit for the two-port technique. In order to further extend the upper frequency limit of the complete CAC model a multi-port technique has been used. The algebra for the multi-ports, based on the admittance relationships between the ports, is derived and presented in an attractive form for easy implementation. Three-dimensional acoustic finite elements have been used to establish the admittance relations for each tank, which is represented by a matrix with the dimensions $(N+1)\times(N+1)$; where N is the number of cooling tubes. The upper frequency limit for this hybrid approach will be defined by the cut-on for the first non-planar mode in the inlet/outlet duct. The highest frequency validated in this particular study is about 1.5 times larger than the cut-on frequency for the tanks while cut-on in the inlet/outlet ducts is outside of the validation frequency band, limited by the experimental set-up. The correspondence between measured and predicted transmission loss is very good in the entire validation band. The suggested technique thereby offers a new possibility to tune the acoustic properties of CACs with respect to frequencies important for breathing noise as well as noise from compressor operation and turbulent flow.

At high engine speed where the mass flow is large the broad band noise generated inside the intake system components due to flow separation might be significant. The A-weighting of the sound pressure level will further enhance the broad band part relative to the low frequency engine harmonic part. Since the turbulent pressure drop of the present CAC is of the same order of magnitude as the rest of the system it will most likely contribute to the total amount of generated flow noise. The model described in this paper only includes the passive properties of the CAC and a future study of the active acoustic part could be of interest.

1.2. Two-port modelling

Assuming a one-dimensional (1D) acoustic state throughout the CAC, the sound propagation can be described using acoustic two-ports [23]. This will be consistent as long as the highest frequency of interest stays well below the cut-on frequency for the first non-planar wave. The frequency domain relationship between the acoustic states at sections representing the inlet and outlet of a two-port can be written

$$\begin{bmatrix} p'_{\text{in}} \\ q'_{\text{in}} \end{bmatrix} = \begin{bmatrix} T_{11} & T_{12} \\ T_{21} & T_{22} \end{bmatrix} \begin{bmatrix} p'_{\text{out}} \\ q'_{\text{out}} \end{bmatrix}, \tag{1}$$

where p' denotes the plane wave acoustic pressure and q' the acoustic volume velocity. For simple generic geometries, such as circular ducts, it is possible to obtain the complex valued components in the transfer matrix from analytical expressions. For a component built up of several sub-components coupled in series, such as a CAC or an after treatment device, the global two-port can be calculated as the product of the individual two-port matrices. For the case of a CAC this can with reference to Fig. 1 be formulated as

$$\mathbf{T}_{\text{CAC}} = \mathbf{T}_{\text{DUCT}}\mathbf{T}_{\text{IN}}\mathbf{T}_{\text{COOL}}\mathbf{T}_{\text{OUT}}\mathbf{T}_{\text{DUCT}}, \tag{2}$$

where the index DUCT corresponds to the inlet/outlet ducts, IN to the inlet tank, COOL to the cooling tubes and OUT to the outlet tank. The two-port matrix $\mathbf{T}_{\text{COOL}}$ for the complete bundle of cooling tubes is obtained from parallel coupling of N tubes via the relation

$$\mathbf{T}_{\text{COOL}} = \begin{bmatrix} T_{11} & T_{12}/N \\ NT_{21} & T_{22} \end{bmatrix}. \tag{3}$$

Here, the matrix components T_{11}, T_{12}, T_{21} and T_{22} represent the data from one single channel. Eq. (2) will be valid only as long as the waves are plane at the sections where the two-ports are coupled together. For the particular case of CACs this will be limited to frequencies well below the cut-on frequency for the section where the cooling tubes enter the inlet or outlet volume. For frequencies above this cut-on frequency, the so-called multi-port technique can be used. The following two sections will describe how the two-ports for

the cooling tubes can be calculated and how a multi-port technique can be implemented in order to extend the valid frequency range for the complete CAC model.

2. Modelling plane waves in narrow tubes

2.1. General

The shortest dimension of the cross-section of a cooling tube in a CAC is of the order of 1–3 mm; hence the sound transmission will be strongly influenced by the viscothermal boundary layers and therefore highly resistive. The typical length of a cooling tube is about 50 cm, and in the case studied here about 70 cm. The ideal choice of model is therefore a two-port where the viscothermal effects are included. A number of such models are available in the literature. One early model for sound propagation in circular tubes is the classical Kirchhoff equation [11] from 1868 that includes the effect of viscosity as well as heat conduction. However, no analytical solution has so far been presented to this complicated transcendental equation. Kirchhoff himself was the first to present an approximate solution to his equation, using the restriction of "wide" ducts, which is the same as large shear wavenumbers. More than 50 years later an approximate solution to a simplified version of Kirchhoff's equation was found by Zwikker and Kosten [12] for circular geometries. Their solution is only dependent on the shear wavenumber and is also known as the "low reduced frequency solution" [13] since it is only valid for cases where $k_0 a \ll 1$ and $k_0 a/s \ll 1$. Here $k_0 = \omega/c_0$, a is the duct radius, c_0 the speed of sound in the fluid, $s = a(\rho_0 \omega/\mu)^{1/2}$ is the shear wavenumber (also known as the Stokes number), ρ_0 the mean density, ω the angular frequency and μ is the dynamic viscosity.

In neither of these early works was the effect of mean flow considered. Inspired by the evolution of catalytic converters, a number of authors have presented improved models accounting for an incompressible mean flow and non-circular geometries [14–19]. For practical applications, the most useful is perhaps the work of Dokumaci [14,15]. In Ref. [14] he showed that the equations for sound propagation in a thermo-viscous fluid, simplified in the manner of Zwikker and Kosten theory [12], could be solved analytically for a circular pipe with a mean flow profile that is constant over the cross-section. In a later paper [15], Dokumaci extended the model in Ref. [14] to include rectangular cross-sections by expanding the solution in terms of a double Fourier sine series. Other works starting out from essentially the same equations as used by Dokumaci [14,15] include Astley and Cummings [16], Peat [17], Ih et al. [18], and Jeong and Ih [19]. At operating conditions, CACs as well as catalytic converters experience temperature and pressure gradients. The effect of axial pressure and temperature gradients has been treated by Peat [20], Peat and Kirby [21], and Dokumaci [22].

The present paper aims to establish an efficient acoustic modelling strategy for CACs where the cross-section of the cooling tubes is irregular and an incompressible mean flow is present. The model that is most suitable for this geometry is probably the model by Astley and Cummings [16], which is based on a finite element discretization of the cross-section of the duct and allows arbitrary geometries. However, the Stokes number for this particular case is larger than for the catalytic converter studied in Ref. [16], which is why a much denser mesh is required which results in longer calculation times. It is of interest to investigate if an analytical model can produce results equivalent to the numerical with a much smaller computational effort. The model by Dokumaci [14] and a modified version of the model by Astley and Cummings [16] are coded and used for this purpose. Since the shape of the propagating profile of the incompressible mean flow can be arbitrary in the model in Ref. [16] a comparison is performed in order to estimate the effects of choosing a plug flow profile instead of a laminar flow profile. The laminar flow profile, which is obtained from the solution to Poisson's equation, is parabolic for the simple case of a circular cross-section and more complicated for other cross-sections. This is indeed interesting since the analytical model in Ref. [14] is based on a plug profile which actually violates the assumption of a laminar flow.

All the models mentioned above assume laminar flow and therefore do not take into account any effect of turbulence on the propagation of sound waves. The transition from laminar to turbulent flow is related to the Reynolds number which for a circular pipe is defined as

$$Re = \frac{U_x D \rho_0}{\mu}, \tag{4}$$

where U_x is the velocity in the axial direction, D the duct diameter, ρ_0 the density and μ the dynamic viscosity. If the cross-section is non-circular but the aspect ratio is not too large, the diameter can be replaced by the hydraulic diameter $D_h = 4S/C$ where S is the cross-section area and C the wetted perimeter. For a circular cross-section transition is known to take place at a Reynolds number just above 2000 [24], but for triangular cross-sections the situation is somewhat more complicated. In the work by Eckert and Irvine [25], it was shown experimentally that transition does not occur simultaneously over the whole of the flow for a channel including a narrow region such as a triangle. For a triangle with an acute angle of 12°, more than 20% of the height is still laminar when the Reynolds number is 4000 (based on the hydraulic diameter).

The mean flow velocity in a CAC, will be defined by the mass flow, temperature, static pressure and the cross-section of the cooling tubes. The area remains of course constant for a particular CAC, but the other three parameters are defined by the operating conditions of the engine and will therefore vary significantly, as will the mean flow. However, in a passenger car the Mach number of the mean flow in the cooling tubes will most likely stay below 0.1 for most driving conditions, except at very high engine revolution speed. The flow regime between a Mach number of 0 and 0.1 will therefore be the most important from the noise point of view. For the particular case of a CAC mounted on a passenger car, the Reynolds number will not be possible to scale just with the mean flow velocity. An increased velocity is the result of the energy added by the compressor wheel which also increases the pressure and the temperature. As the viscosity is dependent on the temperature, and the density on both the temperature and the pressure, it will follow that the Reynolds number will have to be calculated for each load case separately. Representative data taken from both a diesel and a petrol engine at full load conditions will result in Reynolds numbers exceeding 2000. Due to its wider engine speed range the petrol engine will experience Reynolds numbers as high as 8000. At those conditions there will most likely be turbulent flow at least in the major part of the cross-section, which is why a model that takes into account interaction between turbulence and sound waves is required. The model by Howe in Ref. [26] combines the effects of turbulence and viscothermal sub-layers on wave propagations in circular cross-sections. Although it requires the cross-section to be "wide" and the turbulent flow to be fully developed with a constant flow profile, it will provide useful information and understanding concerning the low frequency damping for the cases where the Reynolds number is large. In this paper the model by Howe is applied to create a two-port matrix that includes interaction between turbulence and sound waves. From this two-port transmission loss data is extracted and compared to the corresponding data from the models by Dokumaci [14] and Astley and Cummings [16] for cold conditions as well as hot operating conditions.

2.2. Analytical model including viscothermal effects

The fundamental linearized equations for a viscothermal fluid, as formulated by Zwikker and Kosten [12], describing plane wave propagation in the x-direction, assuming an ideal gas and an incompressible uniform mean flow, are for harmonic time variation [$e^{i\omega t}$], see Ref. [14], as follows:

Conservation of momentum is

$$\rho_0\left(i\omega + U_0\frac{\partial}{\partial x}\right)u'_x = -\frac{\partial p'}{\partial x} + \mu\nabla_S^2 u'_x, \quad p' = p'(x,t). \tag{5}$$

Conservation of mass is

$$\left(i\omega + U_0\frac{\partial}{\partial x}\right)\rho' + \rho_0\nabla\cdot\mathbf{u}' = 0. \tag{6}$$

Conservation of energy is

$$\rho_0 C_p\left(i\omega + U_0\frac{\partial}{\partial x}\right)T' = \left(i\omega + U_0\frac{\partial}{\partial x}\right)p' + \kappa_{th}\nabla_S^2 T'. \tag{7}$$

Using the ideal gas law the following equation of state is obtained as

$$\frac{p'}{p_0} = \frac{\rho'}{\rho_0} + \frac{T'}{T_0}. \tag{8}$$

Here p_0, ρ_0, U_0 and T_0 are the mean pressure, the mean density, the incompressible velocity in the axial direction and the mean temperature, respectively, $\mathbf{u}'$ is the acoustic velocity that comprises u'_x, u'_y and u'_z for each direction, p', ρ' and T' are the acoustic pressure, density and temperature, respectively, C_p is the specific heat at constant pressure, κ_{th} the thermal conductivity and ∇_S^2 is the Laplacian over the cross-section of the cooling tube S. The boundary conditions that must be fulfilled at the duct walls are that no slip is allowed and that temperature fluctuations are negligible. In addition rigid walls are assumed. These conditions imply that $\mathbf{u}' = \mathbf{0}$ and $T' = 0$ on the wall ∂S.

2.2.1. Cylindrical tubes

Following Dokumaci [14] a propagating wave ansatz is assumed

$$p' = p_0 p^* \exp(\mathrm{i}\omega t - \mathrm{i}\Gamma k_0 x), \quad u'_x = p' h(r)/(\rho_0 c_0), \quad T' = p' f(r)/(\rho_0 C_p), \tag{9}$$

where p^* is the dimensionless pressure, k_0 is the wavenumber, $c_0 = (\gamma p_0/\rho_0)^{1/2}$ is the isentropic speed of sound, γ is the ratio of specific heats, Γ is the dimensionless axial propagation constant and r is the radial coordinate. If a circular cross-section is considered the ∇_S^2- and ∇-operators can be transferred to cylindrical coordinates as

$$\nabla_S^2 = \frac{1}{r}\frac{\partial}{\partial r} + \frac{\partial^2}{\partial r^2} \tag{10}$$

and

$$\nabla \cdot \mathbf{u}' = \frac{\partial u'_x}{\partial x} + \frac{\partial u'_r}{\partial r} + \frac{u'_r}{r}. \tag{11}$$

Here u'_r is the acoustic velocity in the radial direction. Substituting Eqs. (9)–(11) into Eq. (5) and (7), while dropping p' from both sides of the equation yields

$$\rho_0(\mathrm{i}\omega - U_0 \mathrm{i}\Gamma k_0)\frac{h}{\rho_0 c_0} = \mathrm{i}\Gamma k_0 + \frac{\mu}{\rho_0 c_0}\left(\frac{1}{r}\frac{\partial h}{\partial r} + \frac{\partial^2 h}{\partial r^2}\right) \tag{12}$$

and

$$(\mathrm{i}\omega - U_0 \mathrm{i}\Gamma k_0) f = (\mathrm{i}\omega - U_0 \mathrm{i}\Gamma k_0) + \frac{\kappa_{\text{th}}}{\rho_0 C_p}\left(\frac{1}{r}\frac{\partial f}{\partial r} + \frac{\partial^2 f}{\partial r^2}\right). \tag{13}$$

Introducing $\beta^2 = \mathrm{i}s^2(1 - \Gamma M)/a^2$ where s is the Stokes number, a the radius of the duct, M the Mach number, and the Prandtl number $\xi^2 = \mu C_p/\kappa_{\text{th}}$, the Eqs. (12) and (13) simplifies to

$$\frac{\partial^2 h}{\partial r^2} + \frac{1}{r}\frac{\partial h}{\partial r} - \beta^2 h = -\frac{\mathrm{i}\Gamma s^2}{a^2} \tag{14}$$

$$\frac{\partial^2 f}{\partial r^2} + \frac{1}{r}\frac{\partial f}{\partial r} - \beta^2 \xi^2 f = -\beta^2 \xi^2 \tag{15}$$

which has the solutions

$$h(r) = C_H J_0(\mathrm{i}\beta r) + \frac{\Gamma}{1 - \Gamma M} \tag{16}$$

and

$$f(r) = C_F J_0(\mathrm{i}\beta\xi r) + 1, \tag{17}$$

where C_H and C_F are constants and J_n is a Bessel function of the first type of order n. The boundary conditions are zero radial acoustic velocity at $r = 0$ and zero acoustic velocity and temperature at the duct wall

$$u'_r(0) = u'_x(a) = u'_r(a) = T'(a) = 0 \tag{18}$$

which yields the solutions

$$h(r) = \frac{\Gamma}{(1-\Gamma M)}\left[1 - \frac{J_0(\mathrm{i}\beta r)}{J_0(\mathrm{i}\beta a)}\right] \tag{19}$$

and

$$f(r) = 1 - \frac{J_0(\mathrm{i}\beta\xi r)}{J_0(\mathrm{i}\beta\xi a)}. \tag{20}$$

Averaging $\langle\ \rangle$ the continuity equation (6) over the cross-section and insertion of Eq. (8) gives

$$\left(\mathrm{i}\omega + U_0\frac{\partial}{\partial x}\right)\left(\frac{\rho_0 p'}{p_0} - \frac{\rho_0\langle T'\rangle}{T_0}\right) + \rho_0\langle\nabla\cdot\mathbf{u}'\rangle = 0. \tag{21}$$

Via Gauss' theorem and by using the boundary conditions in Eq. (18) the last term in Eq. (21) can be rewritten; this yields

$$\left(\mathrm{i}\omega + U_0\frac{\partial}{\partial x}\right)\left(\frac{p'}{p_0} - \frac{\langle T'\rangle}{T_0}\right) + \frac{\partial\langle u_x'\rangle}{\partial x} = 0. \tag{22}$$

Insertion of Eq. (9) and division by p' yields

$$(\mathrm{i}\omega - U_0\mathrm{i}\Gamma k_0)\left(\frac{1}{p_0} - \frac{\langle f\rangle}{\rho_0 C_p T_0}\right) - \frac{\mathrm{i}k_0\Gamma\langle h\rangle}{\rho_0 c_0} = 0 \tag{23}$$

which after some simplifications becomes

$$(1-\Gamma M)\left[1 - \left(1 - \frac{1}{\gamma}\right)\langle f\rangle\right] - \frac{\Gamma\langle h\rangle}{\gamma} = 0. \tag{24}$$

The average of Eq. (19) is

$$\langle h\rangle = \frac{\Gamma}{(1-\Gamma M)}\frac{1}{\pi a^2}\int_0^a\left[1 - \frac{J_0(\mathrm{i}\beta r)}{J_0(\mathrm{i}\beta a)}\right]2\pi r\,\mathrm{d}r = \frac{\Gamma}{(1-\Gamma M)}\left[1 - \frac{2J_1(\mathrm{i}\beta a)}{\mathrm{i}\beta a J_0(\mathrm{i}\beta a)}\right]. \tag{25}$$

The same operation on Eq. (20) yields

$$\langle f\rangle = \left[1 - \frac{2J_1(\mathrm{i}\beta\xi a)}{\mathrm{i}\beta\xi a J_0(\mathrm{i}\beta\xi a)}\right]. \tag{26}$$

Insertion of Eq. (5) and (26) in Eq. (24) yields after some rearrangement

$$(1-\Gamma M)^2\left[1 - \left(1 - \frac{1}{\gamma}\right)G(\mathrm{i}\beta\xi a)\right] - \frac{\Gamma^2}{\gamma}G(\mathrm{i}\beta a) = 0, \tag{27}$$

where

$$G(x) = 1 - \frac{2J_1(x)}{xJ_0(x)}. \tag{28}$$

Eq. (27) can be solved by simple iteration to obtain two roots Γ_1 and Γ_2, representing wave propagation in the positive and negative axial direction, respectively. For the special case of $M = 0$ Eq. (27) simplifies to

$$\left[1 - \left(1 - \frac{1}{\gamma}\right)G(\xi s\sqrt{-\mathrm{i}})\right] - \frac{\Gamma^2}{\gamma}G(s\sqrt{-\mathrm{i}}) = 0 \tag{29}$$

with the solution

$$\Gamma^2 = \frac{1 + (\gamma-1)2J_1(s\xi\sqrt{-\mathrm{i}})/(s\xi\sqrt{-\mathrm{i}}J_0(s\xi\sqrt{-\mathrm{i}}))}{1 - 2J_1(s\sqrt{-\mathrm{i}})/(s\sqrt{-\mathrm{i}}J_0(s\sqrt{-\mathrm{i}}))}. \tag{30}$$

2.2.2. Two-port for circular ducts

In order to establish the two-port matrix the wave admittance $\langle h \rangle/(\rho_0 c_0)$ is used. Eq. (25) yields after some simplifications

$$\frac{\langle h \rangle}{\rho_0 c_0} = \frac{\Gamma G(\mathrm{i}\beta a)}{\rho_0 c_0 (1 - \Gamma M)}. \tag{31}$$

Finally the two-port of one single channel with the length L_p can be calculated as

$$\mathbf{T}_p = \begin{bmatrix} 1 & 1 \\ \dfrac{S\langle h_1 \rangle}{\rho_0 c_0} & \dfrac{S\langle h_2 \rangle}{\rho_0 c_0} \end{bmatrix} \begin{bmatrix} \exp(-\mathrm{i}k_0\Gamma_1 L_p) & \exp(-\mathrm{i}k_0\Gamma_2 L_p) \\ \dfrac{S\langle h_1 \rangle}{\rho_0 c_0}\exp(-\mathrm{i}k_0\Gamma_1 L_p) & \dfrac{S\langle h_2 \rangle}{\rho_0 c_0}\exp(-\mathrm{i}k_0\Gamma_2 L_p) \end{bmatrix}^{-1}, \tag{32}$$

where the indices 1 and 2 denote the two separate roots of Eq. (27). For the case of parallel channels, as in a cooling tube, the two-port $\mathbf{T}_p$ can be calculated using Eq. (32) after multiplication of the capillary area S by the number of channels. Additionally for the case of non-circular geometries, where the aspect ratio of the sides of the tube is not too large, the wave damping of a circular section with the same hydraulic diameter should be a good approximation [27].

2.3. Numerical model including viscothermal effects

For the case of large aspect ratios, the finite element solution scheme formulated by Astley and Cummings [16] can be used in order to further increase the accuracy of the prediction. This formulation will also allow an arbitrary profile of the incompressible mean flow. For the convenience of the reader the derivation of the numerical formulation is partly presented in the section below. The linearized governing equations are the same as was used in Refs. [14,15], here given in Eqs. (5)–(8), with two exceptions. First, in order to eliminate the velocity components perpendicular to the axial direction of the duct, an integral form of the continuity equation (6) is used in combination with the boundary conditions $\mathbf{u}' = \mathbf{0}$ and $T' = 0$ on the wall ∂S. The continuity equation is, without approximation, reformulated to

$$\int_S \left(\left(\mathrm{i}\omega + U_0 \frac{\partial}{\partial x} \right) \rho' + \rho_0 \frac{\partial u_x'}{\partial x} \right) \mathrm{d}S = 0. \tag{33}$$

Secondly, in the derivation by Astley and Cummings [16] the fluctuating part of the dissipation function in the energy equation is retained. However, in the following work this term is excluded in order to simplify the mean flow calculations. The fluctuating dissipation function given in Ref. [16] contains gradients of the mean flow which introduces approximations in the chosen prediction approach. In Section 5.2.1 this omission is justified for this particular case approximated as a circular tube where an analytical solution of the laminar mean flow exists. It should be pointed out that in the derivation of Astley and Cummings the acoustic velocities u_y' and u_z' in the momentum equation are omitted with reference to the work by Peat [17].

2.3.1. Numerical formulation

Following Astley and Cummings [16] a harmonic plane wave type of solution to these equations, where the acoustic variables have been non-dimensionalized using the mean flow quantities and the isentropic speed of sound, can be obtained from the ansatz:

$$u_x' = c_0 u^*(y^*, z^*) \exp(\mathrm{i}\omega t - \mathrm{i}k_0\Gamma x), \tag{34}$$

$$p' = p_0 p^* \exp(\mathrm{i}\omega t - \mathrm{i}k_0\Gamma x), \tag{35}$$

$$T' = T_0 T^*(y^*, z^*) \exp(\mathrm{i}\omega t - \mathrm{i}k_0\Gamma x). \tag{36}$$

Here y^* and z^* are the in-plane non-dimensional coordinates, scaled using half the hydraulic diameter of the cross-section. The cross-sectional area in the non-dimensional y^*–z^* plane is denoted by S^* and its boundary

by ∂S^*. Substitution of Eqs. (34)–(36) into the equation of state (8) and the integrated continuity equation (33) gives

$$\iint_{S^*} [\mathrm{i}(1-\Gamma M)(p^*-T^*)-\mathrm{i}\Gamma u^*]\,\mathrm{d}S^*=0, \tag{37}$$

where $M(y,^* z^*)$ is the Mach number of the incompressible mean flow. The same procedure on the equation for conservation of momentum (5) yields

$$\frac{\gamma}{s^2}\nabla^2_{S^*}u^*-\mathrm{i}\gamma(1-\Gamma M)u^*+\mathrm{i}\Gamma p^*=0, \tag{38}$$

where

$$\nabla^2_{S^*}=\frac{\partial^2}{\partial y^{*2}}+\frac{\partial^2}{\partial z^{*2}} \tag{39}$$

and s is the Stokes' number. The energy equation (7) becomes accordingly

$$\frac{\gamma}{\gamma-1}\frac{1}{s^2\xi^2}\nabla^2_{S^*}T^*-\frac{\gamma}{\gamma-1}\mathrm{i}(1-\Gamma M)T^*+\mathrm{i}(1-\Gamma M)p^*=0, \tag{40}$$

where ξ^2 is the Prandtl number of the fluid.

The finite element process is based on finding an approximate solution (trial solution) of the velocity and temperature fields in the form:

$$u^*=\sum_{i=1}^{n}u_i\phi_i(y,z),\quad T^*=\sum_{i=1}^{n}T_i\phi_i(y,z) \tag{41}$$

where ϕ_i are the known shape functions, which must be able to satisfy the boundary conditions individually, and u_i and T_i are unknown coefficients. The boundary conditions are zero acoustic velocity and temperature at the duct wall

$$u^*=T^*=0\quad \text{on } \partial S^*. \tag{42}$$

The plane wave ansatz for the pressure in Eq. (35) gives

$$p^*=p_1=\text{constant}. \tag{43}$$

Substitution of Eqs. (41) and (43) into the integral equation (37) yields

$$\mathrm{i}S^*(1-\Gamma\bar{M})p^*-\mathrm{i}(\boldsymbol{\varphi}^{\mathrm{T}}-\Gamma\boldsymbol{\varphi}_m^{\mathrm{T}})\mathbf{T}^*-\mathrm{i}\Gamma\boldsymbol{\varphi}^{\mathrm{T}}\mathbf{u}^*=0, \tag{44}$$

where

$$\boldsymbol{\varphi}=\iint_{S^*}\begin{bmatrix}\phi_1\\-\\-\\\phi_n\end{bmatrix}\mathrm{d}S^*,\quad \boldsymbol{\varphi}_m=\iint_{S^*}\begin{bmatrix}M\phi_1\\-\\-\\M\phi_n\end{bmatrix}\mathrm{d}S^*, \tag{45}$$

$$\mathbf{u}^*=\begin{bmatrix}u_1\\-\\-\\u_n\end{bmatrix},\quad \mathbf{T}^*=\begin{bmatrix}T_1\\-\\-\\T_n\end{bmatrix},\quad p^*=[p_1]. \tag{46}$$

The Mach number of the incompressible flow averaged over the cross-section is

$$\bar{M}=\frac{1}{S^*}\iint_{S^*}M(y^*,z^*)\,\mathrm{d}S^*. \tag{47}$$

The method of weighted residuals (known alternatively as the Galerkin procedure) applied to the momentum equation (38), while applying the divergence theorem, yields after some rearrangements

$$\iint_{S^*}\left[-\frac{\gamma}{s^2}\nabla_{S^*}\phi_j\cdot\nabla_{S^*}u^*-\mathrm{i}\gamma(1-\Gamma M)\phi_j u^*+\mathrm{i}\Gamma\phi_j p^*\right]\mathrm{d}S^*=0,\quad j=1,2,\ldots,n. \tag{48}$$

After substitution of the trial functions for p^* and u^* Eq. (48) becomes

$$-\frac{\gamma}{s^2}\mathbf{B}\mathbf{u}^*-\mathrm{i}\gamma[\mathbf{A}-\Gamma\mathbf{A_m}]\mathbf{u}^*+\mathrm{i}\Gamma\boldsymbol{\varphi}p^*=\mathbf{0}. \tag{49}$$

Here $\mathbf{A}$, $\mathbf{B}$ and $\mathbf{A}_m$ are $n\times n$ matrices, where n is the number of nodes and the j–kth components are given by

$$[\mathbf{A}]_{jk}=\iint_{S^*}\phi_j\phi_k\,\mathrm{d}S^*,\quad [\mathbf{B}]_{jk}=\iint_{S^*}\nabla_{S^*}\phi_j\cdot\nabla_{S^*}\phi_k\,\mathrm{d}S^*, \tag{50}$$

$$[\mathbf{A}_m]_{jk}=\iint_{S^*}M\phi_j\phi_k\,\mathrm{d}S^*. \tag{51}$$

The same procedure can be used for the energy equation (40)

$$-\frac{\gamma}{\gamma-1}\frac{1}{s^2\xi^2}\mathbf{B}\mathbf{T}^*-\mathrm{i}\frac{\gamma}{\gamma-1}[\mathbf{A}-\Gamma\mathbf{A}_m]\mathbf{T}^*+\mathrm{i}[\boldsymbol{\varphi}-\Gamma\boldsymbol{\varphi}_m]p^*=\mathbf{0}. \tag{52}$$

Eqs. (44), (49) and (52) have to be solved together, which is most easily visualized as the matrix equation

$$\left[\begin{bmatrix}\mathrm{i}S^* & \mathbf{0} & -\mathrm{i}\boldsymbol{\varphi}^{\mathrm{T}}\\ \mathbf{0} & \gamma\mathbf{B}/s^2+\mathrm{i}\gamma\mathbf{A} & \mathbf{0}\\ -\mathrm{i}\boldsymbol{\varphi} & \mathbf{0} & \dfrac{\gamma}{\gamma-1}\left[\dfrac{\mathbf{B}}{s^2\xi^2}+\mathrm{i}\mathbf{A}\right]\end{bmatrix}-\Gamma\begin{bmatrix}\mathrm{i}S^*\bar{M} & \mathrm{i}\boldsymbol{\varphi}^{\mathrm{T}} & -\mathrm{i}(\boldsymbol{\varphi}_m)^{\mathrm{T}}\\ \mathrm{i}\boldsymbol{\varphi} & \mathrm{i}\gamma\mathbf{A}_m & \mathbf{0}\\ -\mathrm{i}\boldsymbol{\varphi}_m & \mathbf{0} & \dfrac{\gamma}{\gamma-1}\mathrm{i}\mathbf{A}_m\end{bmatrix}\right]\begin{bmatrix}p^*\\ \mathbf{u}^*\\ \mathbf{T}^*\end{bmatrix}=\begin{bmatrix}0\\ \mathbf{0}\\ \mathbf{0}\end{bmatrix}. \tag{53}$$

Here $\mathbf{0}$ indicates a zero matrix of appropriate size. For the case of zero mean flow, $\bar{M}=0$, all sub-matrices with index m are zero. The eigenvalue problem in Eq. (53) will only contain two non-trivial roots having the same values but opposite sign. As can be observed from the ansatz (35) they represent wave propagation in positive and negative axial direction with equal speed and attenuation. For the case of a present mean flow a full set of non-trivial eigenvalues will exist. As discussed in Ref. [16] two of those will behave almost like the solutions in the no-flow case. Only those two modes will be retained in the present work.

Axi-symmetric modelling of a circular cross-section is simplified with a 1D approach where the same equations are formulated using cylindrical coordinates. The variables u^* and T^* in Eqs. (34) and (36) are only dependent on the non-dimensional radial coordinate r^* and the operator $\nabla^2_{S^*}$ is transferred to $\{\partial^2/\partial r^{*2}+(1/r)\partial/\partial r^*\}$.

2.3.2. Two-port calculation

The eigenvectors corresponding to the above-mentioned two eigenvalues describe the shape of the profile of the propagating acoustic variables in the axial direction and can be rewritten as

$$\boldsymbol{\Lambda}_j=\begin{bmatrix}\Lambda_{pj}\\ \boldsymbol{\Lambda}_{uj}\\ \boldsymbol{\Lambda}_{Tj}\end{bmatrix}, \tag{54}$$

where Λ_{pj}, $\boldsymbol{\Lambda}_{uj}$ and $\boldsymbol{\Lambda}_{Tj}$ denotes the eigenvector for the pressure, velocity and temperature respectively, taken for eigenvector j. Since the pressure is assumed to be constant over the cross-section Λ_p is a single value while $\boldsymbol{\Lambda}_u$ and $\boldsymbol{\Lambda}_T$ are vectors of size $n\times 1$. In order to establish a two-port for the duct the dimensional axial acoustic velocity u'_x has to be averaged over the cross-section. For this purpose, the shape functions in Eq. (45) can conveniently be used:

$$\langle u'_x\rangle=\frac{c_0\boldsymbol{\varphi}^{\mathbf{T}}\boldsymbol{\Lambda}_u}{S^*}. \tag{55}$$

The averaged admittance is thereafter calculated using Eq. (55) and the pressure from Eq. (35) as

$$\frac{\langle h\rangle}{\rho_0 c_0}=\frac{c_0\boldsymbol{\varphi}^{\mathbf{T}}\boldsymbol{\Lambda}_u}{p_0\Lambda_p S^*}. \tag{56}$$

Using the definition for speed of sound, Eq. (56) simplifies to

$$\frac{\langle h\rangle}{\rho_0 c_0}=\frac{\gamma\boldsymbol{\varphi}^{\mathbf{T}}\boldsymbol{\Lambda}_u}{\rho_0 c_0\Lambda_p S^*}. \tag{57}$$

Finally, $\langle h\rangle$ and Γ for the two acoustic modes is substituted into Eq. (32), upon maintaining their signs, to establish the desired two-port for the tube-element.

2.3.3. Numerical formulation of the mean flow

The establishment of the matrices $\mathbf{A}_m$ and $\boldsymbol{\varphi}_m$ requires the mean flow to be known at all positions in the cross-section. The laminar flow profile for the non-dimensionalized cross-section can be obtained from the solution to Poisson's equation [16] as

$$\frac{\partial^2 M}{\partial y^{*2}}+\frac{\partial^2 M}{\partial z^{*2}}=\frac{a^2 G}{\mu c_0}, \tag{58}$$

where G is the (dimensional) pressure gradient of the incompressible steady flow in the axial direction and a half the hydraulic diameter of the cross-section. The solution scheme of this equation is obtained using the same procedure as was used for the conservation of momentum and energy. The Galerkin process, the divergence theorem and the boundary condition ($M=0$) on the tube wall ∂S^* yields after some rearrangements:

$$\iint_{S^*}\left[\nabla_{S^*}\phi_j\cdot\nabla_{S^*}M+\frac{a^2 G}{\mu c_0}\phi_j\right]\mathrm{d}S^*=0,\quad j=1,2,\ldots,n, \tag{59}$$

The trial functions for the Mach number are on the same form as those that were used for the velocity and temperature

$$M=\sum_{i=1}^{n}M_i\phi_i(y^*,z^*). \tag{60}$$

Substitution of Eq. (60) into Eq. (59) yields

$$\mathbf{B}\mathbf{M}+\frac{a^2 G}{\mu c_0}\boldsymbol{\varphi}=0, \tag{61}$$

where

$$\mathbf{M}=\begin{bmatrix}M_1\\-\\-\\M_n\end{bmatrix} \tag{62}$$

and $\mathbf{B}$ is defined in Eq. (50) and $\boldsymbol{\varphi}$ in Eq. (45). The mean flow $\bar{M}$ can finally be calculated from Eq. (47) using the shape functions in the same way as in Eq. (55).

2.3.4. Calculation of the shape functions

The derivation of the shape functions is straightforward and well documented in several text books (see for instance the book by Zienkiewicz and Taylor [33]). The finite element discretization in this work is performed using nine-noded isoparameteric Lagrangian rectangular elements. Nine-point Gauss–Legendre integration is used to evaluate the element integrals $\mathbf{A}$, $\mathbf{B}$, $\boldsymbol{\varphi}$, $\mathbf{A}_m$ and $\boldsymbol{\varphi}_m$ at the Gauss points. The information about the Mach number of the incompressible mean flow is used when evaluating $\mathbf{A}_m$ and $\boldsymbol{\varphi}_m$ at the integration points. If the same element discretization is used for the mean flow problem as for the acoustic problem, the data is

calculated only at the node points and 2D interpolation must be used in order to predict the Mach number at the Gauss points.

2.4. Analytical model including effects of turbulence

When a turbulent flow is present the acoustic waves will be attenuated due to transfer of energy to turbulent stresses if the thickness of the acoustic boundary layer, $\delta_{ac} = (2\nu/\omega)^{1/2}$, is larger than that of the viscous sub-layer of the turbulent mean flow boundary layer, $\delta_v \approx 10\nu/(\tau_w/\rho_0)^{1/2}$, [28,29]. Here, ν denotes the kinematic viscosity, ρ_0 the density of the fluid and τ_w the mean wall shear stress. Introducing the friction velocity as $u_* = (\tau_w/\rho_0)^{1/2}$, the viscous sub-layer is $\delta_v \approx 10\nu/u_*$. An early effort addressing damping of sound waves in the presence of flow was made by Ingard and Singhal [30]. More recent work include Peters et al. [29] and Howe [26] where the latest is the most complete model developed so far [31].

Howe [26] proposed a frequency dependent model for the turbulent boundary layer eddy viscosity controlling the momentum and thermal boundary layers, which are formed from interaction between turbulent boundary layers and sound waves. The model is restricted to cases with fully developed and low Mach number ($M<0.1$) turbulent flow and only treats one-dimensional axial wave propagation. It is strictly valid for situations where the thickness of the turbulent boundary layer is much smaller than the acoustic wavelength so that the layers can be described by an effective acoustic admittance. The model has so far proven to provide good agreement with experimental data from Peters et al. [29] for Reynolds numbers exceeding 10^4, which is well above the transition which normally takes place just above a Reynolds number of 2000, based on the hydraulic diameter [24,25]. These circumstances justify the simplification that the profile of the mean flow is regarded as uniform in the core of the flow.

2.4.1. Circular tubes

The acoustic wave is once again given by the ansatz

$$p' = p_0 p^* \exp(\mathrm{i}\omega t - \mathrm{i}\Gamma k_0 x). \tag{63}$$

The propagation constant, corrected for turbulent flow, is given by Howe [26] as

$$\Gamma = \pm\frac{1}{1\pm M} \mp \frac{2\mathrm{i}\rho_0 c_0}{(1\pm M)D_h k_0}\, Y_C\left(\frac{\pm k_0}{1\pm M}, \omega\right). \tag{64}$$

Here, Y_C is the complex conjugate of the boundary layer admittance Y which is calculated as

$$Y(k,\omega) = \frac{\mathrm{e}^{-\mathrm{i}\pi/4}}{\rho_0\omega^{3/2}}\left[k^2\sqrt{\nu}F_A\left(\sqrt{\frac{\mathrm{i}\omega\nu}{\kappa^2 u_*^2}}, \delta_v\sqrt{\frac{\mathrm{i}\omega}{\nu}}\right) + \frac{\beta\omega^2}{c_p}\sqrt{\chi}F_A\left(\sqrt{\frac{\mathrm{i}\omega\chi P_t^2}{\kappa^2 u_*^2}}, \delta_v\sqrt{\frac{\mathrm{i}\omega}{\chi}}\right)\right], \tag{65}$$

where $\kappa \approx 0.41$ is the von Karman constant, P_t is a turbulence Prandtl number, assumed to be constant and equal to 0.7 for air [26], $\chi = \kappa_{th}/(\rho_0 C_p)$ is the thermometric conductivity, which for air at 20 °C is about $2\times10^5\,\mathrm{m^2\,s^{-1}}$. Moreover, the function F_A is defined as

$$F_A(a,b) = \frac{\mathrm{i}\left[H_1^{(1)}(a)\cos(b) - H_0^{(1)}(a)\sin(b)\right]}{H_0^{(1)}(a)\cos(b) - H_1^{(1)}(a)\sin(b)}, \tag{66}$$

where $H_n^{(1)}$ is a Hankel function of order n. The friction velocity is calculated from the empirical pipe flow formula

$$U_0/u_* = 2.44\ln(u_* D_h/2\nu) + 2.0. \tag{67}$$

Finally, the thickness of the viscous sub-layer is calculated using the empirical formula [26]

$$\frac{\delta_v u_*}{\nu} = 6.5\left(1 + \frac{1.7(\omega/\omega_*)^3}{1+(\omega/\omega_*)^3}\right), \quad \omega_*\nu/u_*^2 \approx 0.01, \quad \omega > 0. \tag{68}$$

Here, ω_* is the critical frequency representing the centre of the range where the principal acoustic–turbulence interaction occurs in a close-to-the-wall region where viscous as well as turbulence diffusion is significant.

2.4.2. Two-port for circular tubes

In order to extend Howe's model to enable extraction of a two-port for a circular duct the wave admittance $\langle h \rangle/(\rho_0 c_0)$ is required. This can be calculated using the axial momentum conservation equation where the velocity has been averaged over the cross-section,

$$\frac{D\langle u'_x \rangle}{Dt} + \frac{1}{\rho_0}\frac{\partial p'}{\partial x} = 0, \tag{69}$$

where $D/Dt \equiv \partial/\partial t + U_0 \partial/\partial x$. Assuming harmonic waves yields the wave admittance as

$$\frac{\langle u'_x \rangle}{p'} = \frac{\langle h \rangle}{\rho_0 c_0} = \frac{\Gamma}{\rho_0 c_0 (1 - \Gamma M)}. \tag{70}$$

The two-port for the duct can thereafter be obtained from substituting the expressions for $\langle h \rangle$ and Γ into Eq. (32). As for the two previously described models, there exist two solutions for propagation in opposite directions, in Eq. (32) denoted by the indices 1 and 2. Both are required for the two-port extraction and the appropriate sign will follow from the two solutions for Γ, obtained from Eq. (64).

3. Modelling a complete charge air cooler

3.1. General

The charge air cooler used in this study is taken from a passenger car in series production and is used for diesel as well as petrol engines. It is assembled from several parts made of different materials. The cooler is of brick type with relatively compact dimensions, which makes it suitable for densely packed engine compartments. There are ten cooling tubes made of aluminium, each of them divided into 36 channels due to the turbulator installation, as shown in Fig. 4. The air is prevented from flowing between the channels and there is no flow reversal taking place inside the cooler. The cooling tubes are modelled using the two-ports that were extracted using the techniques described in Section 2.

3.2. In- and outlet sections

The inlet tank consists of a 90° bend and a diverging conical section connecting the inlet duct to the cooling tubes. The walls are made of plastic and are reinforced by some ribs in order to reduce vibrations as well as sound transmission. The total cross-sectional area of the ten cooling tubes is about 50% larger than that of the inlet duct. This is a good way to compensate for the larger pressure drop present in the narrow cooling tubes. In order to create a good flow for the cold air outside the cooling tubes, and thereby an efficient heat transfer from the charged air inside the CAC to the cooling air, there is a slit separating each tube from its neighbour. This geometrical separation of the tubes makes the area at the largest section of the inlet tank more than twice that of the cooling tubes. The geometry of the outlet tank is almost symmetric to that of the inlet, of course with the restriction that the mean flow here is contracted. The acoustics of such conical devices (horns) has been treated by several authors where the most recent publications have addressed the effect of flow. Approximate plane wave models based on series of straight ducts have been discussed by Åbom [32], for example, who showed that only a few segments are required to create very good results.

3.2.1. 3D finite element models

In order to extend the valid frequency range and include cross-modes, for such complicated geometries as the tanks, acoustic finite elements can be used. Most commercial finite element software packages include 3D linear acoustic finite elements (FE) and there are a large number of textbooks describing the

theory (see e.g. Ref. [33]); therefore it will not be further described here. In the 3D FE-calculations in the present work LMS/Sysnoise [34] has been used. In this code the convective effect of a superimposed incompressible mean flow can easily be accounted for, although it has been neglected here due to the small Mach number that remains from the large expansion. Some codes also allow the use of admittance matrices to connect two different volumes using the acoustic velocity and pressure as coupling variables [34]. This procedure requires the complete model to be solved for each frequency for each load case, which is time consuming as well as expensive for models with fine element resolution. A good method to shorten iteration time, if the properties of the air mixture and the geometry of the tanks are fixed, is to use the multi-port approach that will be described in the next section.

The tanks of the charge air cooler used in this study are very similar in size and shape. The volume of the inlet tank is 853 cm^3 and that of the outlet tank is 896 cm^3. There is a circular opening in the wall of the outlet tank designed to support a temperature transducer. In all measurements and calculation results presented here this hole is carefully plugged to create a smooth wall. In order to achieve a fast and simple meshing procedure, linear tetrahedral elements with four nodes are used to model the volumes and linear wedge element with six nodes for the pipes. The use of hexahedral elements with eight nodes would certainly be more efficient but the process of creating the element mesh is still not possible to fully automate and hence very cumbersome. Parabolic tetrahedral elements would of course also be an efficient choice but for this case it was decided to use the linear element with very high resolution. The chosen element size is 5 mm which yields more than 40 elements per wavelength for analyses performed at a frequency of 1600 Hz at cold conditions and more than 50 for the warmer air present at full load and medium engine speed. The total number of nodes is about 23 000 in each tank, built up using 76 000 elements in the inlet tank and 83 000 in the outlet tank. This finite element mesh is shown in Fig. 5.

The circular pipes connecting the tanks to the rest of the gas exchange ducting of the engine have diameters equal to 60 mm. Short parts of the measurement ducts, with a diameter 66 mm, are also included in the model in order to make sure that the waves are plane after the 90° bend in each tank. The same technique is also used at the connection to the cooling tubes where acoustical near fields are present due to the sudden contraction and expansion.

When using acoustical finite elements it is well known that the numerical integration of the pressure at a boundary is performed exactly. However, the acoustic velocity boundary condition is obtained only in a weak sense since it is of Neumann type. The prediction of the acoustic velocity at a boundary is obtained from extrapolation of the results at the integration points inside the elements to the boundary. To account for the inaccuracy resulting from the extrapolation, the elements at all openings are made extremely short (0.1 mm).

To simulate the effect of yielding walls and propagation losses in the inlet and outlet sections, made of plastic, damping is applied as a complex speed of sound. Based on the investigation by Knutsson et al. in Ref. [35], an engineering estimate for the damping in intake system components made of plastic is obtained by setting the imaginary part of the speed of sound equal to 1% of the real part.

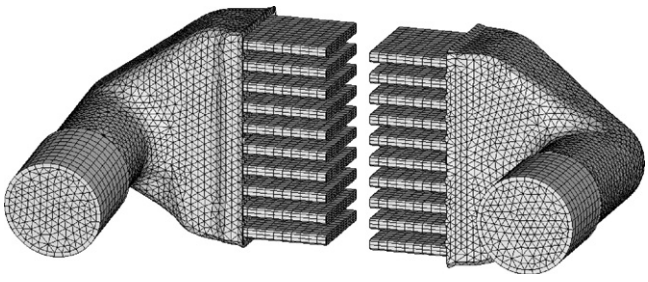

Fig. 5. Finite element mesh of inlet and outlet tanks (the tanks have been moved together in the image).

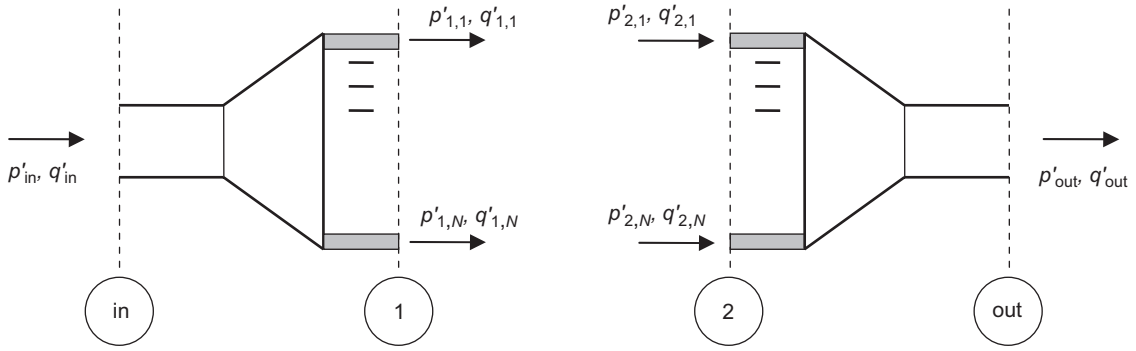

Fig. 6. Definition of acoustic variables at multi-port openings.

3.2.2. Multi-port mobility matrices

The acoustics of the tank volumes of the CAC can be represented by the admittance matrix relations $\mathbf{A}_{\text{Tn}}$, which relates the acoustic volume velocities q' to the pressures p' at all openings as

$$\begin{bmatrix} q'_{\text{in}} \\ \mathbf{q}'_1 \end{bmatrix} = [\mathbf{A}_{\text{T1}}] \begin{bmatrix} p'_{\text{in}} \\ \mathbf{p}'_1 \end{bmatrix}, \quad \begin{bmatrix} q'_{\text{out}} \\ \mathbf{q}'_2 \end{bmatrix} = [\mathbf{A}_{\text{T2}}] \begin{bmatrix} p'_{\text{out}} \\ \mathbf{p}'_2 \end{bmatrix}, \tag{71}$$

where the indices in and out represent the in- and outlet of the two-port for the complete CAC, T1 and T2 are the inlet and outlet tank respectively. The vectors $\mathbf{q}'_1$ and $\mathbf{p}'_1$ are of size $N \times 1$ and represent the acoustic volume velocities and pressures, respectively at the inlets to the cooling tubes. Here N is the number of cooling tubes. The vectors $\mathbf{q}'_2$ and $\mathbf{p}'_2$ represent the corresponding variables at the outlets from the cooling tubes into the outlet tank. The direction of all volume velocities are with reference to Fig. 6.

The admittance coupling between the inlet and outlet of one cooling tube can be expressed as

$$\begin{bmatrix} q'_1 \\ q'_2 \end{bmatrix} = \begin{bmatrix} M_{p,11} & M_{p,12} \\ M_{p,21} & M_{p,22} \end{bmatrix} \begin{bmatrix} p'_1 \\ p'_2 \end{bmatrix}, \tag{72}$$

where the indices 1 and 2 represent the inlet and outlet of the cooling tube. The admittance matrix can be expanded in order to include the complete bundle of cooling tubes as

$$\begin{bmatrix} \mathbf{q}'_1 \\ \mathbf{q}'_2 \end{bmatrix} = \begin{bmatrix} M_{p,11} & 0 & . & . & 0 & M_{p,12} & 0 & . & . & 0 \\ 0 & M_{p,11} & . & . & . & 0 & M_{p,12} & . & . & . \\ . & . & . & . & . & . & . & . & . & . \\ . & . & . & . & 0 & . & . & . & . & 0 \\ 0 & . & . & 0 & M_{p,11} & 0 & . & . & 0 & M_{p,12} \\ M_{p,21} & 0 & . & . & 0 & M_{p,22} & 0 & . & . & 0 \\ 0 & M_{p,21} & . & . & . & 0 & M_{p,22} & . & . & . \\ . & . & . & . & . & . & . & . & . & . \\ . & . & . & . & 0 & . & . & . & . & 0 \\ 0 & . & . & 0 & M_{p,21} & 0 & . & . & 0 & M_{p,22} \end{bmatrix} \begin{bmatrix} \mathbf{p}'_1 \\ \mathbf{p}'_2 \end{bmatrix}. \tag{73}$$

The admittance matrix above can also be written in a more compact form as:

$$\mathbf{M}_p^{\text{tot}} = \begin{bmatrix} \mathbf{E}M_{p,11} & \mathbf{E}M_{p,12} \\ \mathbf{E}M_{p,21} & \mathbf{E}M_{p,22} \end{bmatrix} = \begin{bmatrix} \mathbf{M}_{p,11} & \mathbf{M}_{p,12} \\ \mathbf{M}_{p,21} & \mathbf{M}_{p,22} \end{bmatrix}, \tag{74}$$

where $\mathbf{E}$ is a unity matrix of size $N \times N$. The matrices $\mathbf{A}_{T1}$ and $\mathbf{A}_{T2}$ can be divided into sub-matrices as

$$[\mathbf{A}] = \begin{bmatrix} A_{11} & \mathbf{a}^r \\ \mathbf{a}^c & \mathbf{A}' \end{bmatrix}, \tag{75}$$

where $\mathbf{A}'$ is a matrix of order $N \times N$ where the first row and column in the matrix $\mathbf{A}$ has been excluded, $\mathbf{a}^r$ and $\mathbf{a}^c$ are vectors of length N representing, respectively the previously excluded first row and column in $\mathbf{A}$ except the first position which here is denoted A_{11}. Hereafter Eq. (73) can be assembled into Eq. (71) which results in the following systems of equations

$$\begin{cases} q'_{\text{in}} = A_{T1,11} p'_{\text{in}} + \mathbf{a}^r_{T1} \mathbf{p}'_1 \\ \mathbf{M}_{p,11} \mathbf{p}'_1 + \mathbf{M}_{p,12} \mathbf{p}'_2 = \mathbf{a}^c_{T1} p'_{in} + \mathbf{A}'_{T1} \mathbf{p}'_1 \end{cases} \tag{76}$$

and

$$\begin{cases} q'_{\text{out}} = A_{T2,11} p'_{\text{out}} + \mathbf{a}^r_{T2} \mathbf{p}'_2 \\ \mathbf{M}_{p,21} \mathbf{p}'_1 + \mathbf{M}_{p,22} \mathbf{p}'_2 = \mathbf{a}^c_{T2} p'_{\text{out}} + \mathbf{A}'_{T2} \mathbf{p}'_2 \end{cases}. \tag{77}$$

The last equations in system (76) and (77) yields $\mathbf{p}'_1$ and $\mathbf{p}'_2$ as

$$\mathbf{p}'_1 = \underbrace{-[\mathbf{M}_{p,11} - \mathbf{A}'_{T1}]^{-1} \mathbf{M}_{p,12}}_{\mathbf{B}_1} \mathbf{p}'_2 + \underbrace{[\mathbf{M}_{p,11} - \mathbf{A}'_{T1}]^{-1} \mathbf{a}^c_{T1}}_{\mathbf{b}^c_1} p'_{\text{in}} \tag{78}$$

and

$$\mathbf{p}'_2 = \underbrace{-\left[\mathbf{M}_{p,22} - \mathbf{A}'_{T2}\right]^{-1} \mathbf{M}_{p,21}}_{\mathbf{B}_2} \mathbf{p}'_1 + \underbrace{\left[\mathbf{M}_{p,22} - \mathbf{A}'_{T2}\right]^{-1} \mathbf{a}^c_{T2}}_{\mathbf{b}^c_2} p'_{\text{out}} \tag{79}$$

respectively. Substitution of Eq. (78) into (79) yields, after some rearrangements

$$\mathbf{p}'_2 = (\mathbf{E} - \mathbf{B}_2 \mathbf{B}_1)^{-1} \mathbf{B}_2 \mathbf{b}^c_1 p'_{\text{in}} + (\mathbf{E} - \mathbf{B}_2 \mathbf{B}_1)^{-1} \mathbf{b}^c_2 p'_{\text{out}}. \tag{80}$$

This expression is used in Eq. (78) to obtain $\mathbf{p}'_1$ as

$$\mathbf{p}'_1 = (\mathbf{B}_1 (\mathbf{E} - \mathbf{B}_2 \mathbf{B}_1)^{-1} \mathbf{B}_2 + \mathbf{E}) \mathbf{b}^c_1 p'_{\text{in}} + \mathbf{B}_1 (\mathbf{E} - \mathbf{B}_2 \mathbf{B}_1)^{-1} \mathbf{b}^c_2 p'_{\text{out}}. \tag{81}$$

Finally, Eqs. (80) and (81) are substituted into the first expressions in Eqs. (76) and (77) to obtain the admittance matrix for the complete CAC unit, $\mathbf{A}_{CAC}$. After some simplifications this relation can be expressed as

$$\begin{bmatrix} q'_{\text{in}} \\ q'_{\text{out}} \end{bmatrix} = \begin{bmatrix} A_{T1,11} + \mathbf{a}^r_{T1} (\mathbf{B}_1 \mathbf{B} \mathbf{B}_2 + \mathbf{E}) \mathbf{b}^c_1 & \mathbf{a}^r_{T1} \mathbf{B}_1 \mathbf{B} \mathbf{b}^c_2 \\ \mathbf{a}^r_{T1} \mathbf{B} \mathbf{B}_2 \mathbf{b}^c_1 & A_{T1,11} + \mathbf{a}^r_{\text{out}} \mathbf{B} \mathbf{b}^c_2 \end{bmatrix} \begin{bmatrix} p'_{\text{in}} \\ p'_{\text{out}} \end{bmatrix}, \tag{82}$$

where $\mathbf{B} = (\mathbf{E} - \mathbf{B}_2 \mathbf{B}_1)^{-1}$. The admittance matrix, that is now of the order 2×2 since there are only two ports on the component, can easily be transformed to the transfer-matrix format as

$$T_{CAC} = \frac{1}{A_{CAC,21}} \begin{bmatrix} -A_{CAC,22} & 1 \\ A_{CAC,12} A_{CAC,21} - A_{CAC,11} A_{CAC,22} & A_{CAC,11} \end{bmatrix}. \tag{83}$$

To establish the admittance matrices for the tanks in Eq. (71) $N+1$ load cases are required. These are composed by using identical FE models but with different boundary conditions. The relation between the admittance matrix and the calculated acoustic volume velocities and pressures at the 11 ports for the inlet tank is

$$\begin{bmatrix} q'_{\text{in}-LC1} & q'_{\text{in}-LC2} & \cdots & q'_{\text{in}-LC11} \\ \mathbf{q}'_{1-LC1} & \mathbf{q}'_{1-LC2} & \cdots & \mathbf{q}'_{1-LC11} \end{bmatrix} = [\mathbf{A}_{T1}] \begin{bmatrix} p'_{\text{in}-LC1} & p'_{\text{in}-LC2} & \cdots & p'_{\text{in}-LC11} \\ \mathbf{p}'_{1-LC1} & p'_{\text{in}-LC2} & \cdots & \mathbf{p}'_{1-LC11} \end{bmatrix}, \tag{84}$$

where $q'_{\text{in}-LCn}$ and $p'_{\text{in}-LCn}$ represent the resulting acoustic volume velocity and pressure for load case n and the vectors $\mathbf{q}'_{1-LCn}$ and $\mathbf{p}'_{1-LCn}$, of size $N \times 1$, contain the corresponding values at the cooling tube inlets.

The admittance matrix is obtained from the product of the matrix containing the volume velocities and the inverted pressure matrix. The corresponding matrix for the outlet tank is obtained accordingly, directions of the acoustic volume velocities with reference to Fig. 6.

3.2.3. Compensation for near field effects at multi-port openings

The 3D FE models of the tanks include a short part of the cooling tubes in order to establish a plane wave at the boundary of the multi-port. The FE formulation does not take into account any effects of boundary layers or turbulence in those narrow parts and as a result these will be missing in the final two-port. An approximate method to reintroduce the missing damping is to assume plane waves in the tubular parts of the tank-model, virtually transfer the position of the multi-port openings back to the section where the tubes enter the tank, and use the full length in the two-ports for the tubes. The formalism for this will be described below.

The relation between the acoustic variables at position 1 and 1A, where 1A is the new position for the tube ports, can be described using Eq. (1) as

$$\begin{bmatrix} p'_1 \\ q'_1 \end{bmatrix}_n = \begin{bmatrix} T_{11} & T_{12} \\ T_{21} & T_{22} \end{bmatrix} \begin{bmatrix} p'_{1A} \\ q'_{1A} \end{bmatrix}_n, \tag{85}$$

where $n = 1, 2, \ldots, N$. For a straight duct the transfer matrix is

$$\begin{bmatrix} T_{11} & T_{12} \\ T_{21} & T_{22} \end{bmatrix} = \mathrm{e}^{-\mathrm{i}kML/(1-M^2)} \begin{bmatrix} \cos(kL_A/(1-M^2)) & \mathrm{i}Z\sin(kL_A/(1-M^2)) \\ (\mathrm{i}/Z)\sin(kL_A/(1-M^2)) & \cos(kL_A/(1-M^2)) \end{bmatrix}, \tag{86}$$

where k is the wavenumber, M the Mach number and Z the wave impedance; all three taken for one single tube in the FE model. L_A is the translation distance which will be negative for the inlet tank and positive for the outlet. Eq. (85) can be rewritten, in order to represent all the ten cooling tubes, as

$$\begin{bmatrix} \mathbf{p}'_1 \\ \mathbf{q}'_1 \end{bmatrix} = \begin{bmatrix} T_{11}\mathbf{E} & T_{12}\mathbf{E} \\ T_{21}\mathbf{E} & T_{22}\mathbf{E} \end{bmatrix} \begin{bmatrix} \mathbf{p}'_{1A} \\ \mathbf{q}'_{1A} \end{bmatrix}, \tag{87}$$

where $\mathbf{E}$ once again is a unity matrix of size $N \times N$. Substitution of Eq. (87) into Eq. (71) yields

$$\begin{cases} q'_{\mathrm{in}} = A_{11}p'_{\mathrm{in}} + \mathbf{a}_r(\mathbf{T}_{11}\mathbf{p}'_{1A} + \mathbf{T}_{12}\mathbf{q}'_{1A}) \\ (\mathbf{T}_{21}\mathbf{p}'_{1A} + \mathbf{T}_{22}\mathbf{q}'_{1A}) = \mathbf{a}_c\mathbf{p}'_{in} + \mathbf{A}'(\mathbf{T}_{11}\mathbf{p}'_{1A} + \mathbf{T}_{12}\mathbf{q}'_{1A}), \end{cases} \tag{88}$$

where $\mathbf{T}_{ij} = T_{ij}\mathbf{E}$. These expressions can thereafter be used to establish an admittance relation between q'_{in}, $\mathbf{q}'_{1A}$, p'_{in}, and $\mathbf{p}'_{1A}$ on the same form as Eq. (71). The expression for $\mathbf{q}'_{1A}$ is

$$\mathbf{q}'_{1A} = \underbrace{[\mathbf{T}_{22} - \mathbf{A}'\mathbf{T}_{12}]^{-1}[\mathbf{A}'\mathbf{T}_{11} - \mathbf{T}_{21}]}_{\mathbf{F}_1}\mathbf{p}'_{1A} + \underbrace{[\mathbf{T}_{22} - \mathbf{A}'\mathbf{T}_{12}]^{-1}\mathbf{a}_c}_{\mathbf{f}_1^c}p'_{\mathrm{in}} \tag{89}$$

which thereafter is used to obtain q'_{in}. After some simplifications this expression becomes

$$q'_{\mathrm{in}} = [A_{11} + \mathbf{a}_r\mathbf{T}_{12}\mathbf{f}_1^c]p'_{\mathrm{in}} + [\mathbf{a}_r\mathbf{T}_{11} + \mathbf{a}_r\mathbf{T}_{12}\mathbf{F}_1]\mathbf{p}'_{1A}. \tag{90}$$

Finally the admittance matrix for a multi-port where the ports have been translated becomes

$$\begin{bmatrix} q'_{\mathrm{in}} \\ \mathbf{q}'_{1A} \end{bmatrix} = \begin{pmatrix} A_{11} + \mathbf{a}_r\mathbf{T}_{12}\mathbf{f}_1^c & \mathbf{a}_r(\mathbf{T}_{11} + \mathbf{T}_{12}\mathbf{F}_1) \\ \mathbf{f}_1^c & \mathbf{F}_1 \end{pmatrix} \begin{bmatrix} p'_{\mathrm{in}} \\ \mathbf{p}'_{1A} \end{bmatrix} \tag{91}$$

which will be used to represent the inlet tank instead of Eq. (71). The procedure to obtain the admittance matrix for the outlet tank is identical.

3.3. Acoustic coupling at cross-section discontinuities

At the outlet from each cooling tube there is an abrupt expansion (see Fig. 7a), which needs a separate two-port for the cases when there is a mean flow present. Flow separation will be present; hence, entropy is

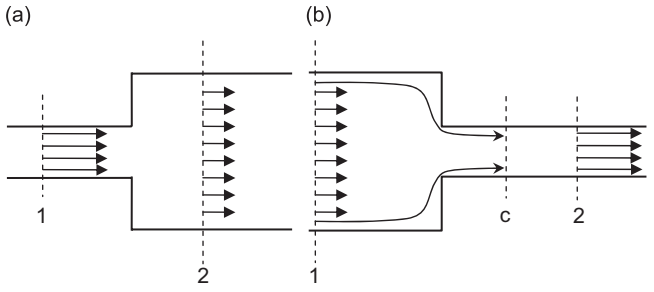

Fig. 7. Mean flow velocity profiles at (a) area expansion and (b) area contraction.

generated due to the dissipation in the turbulent mixing region downstream the flow separation. This interaction between the acoustic field and the flow separation is, however, very complex and complete analytical models are complicated. An example of such a model is the work by Boij and Nilsson [36]. Several authors have suggested models based on simplified velocity fields. The model used here is based on the simple analysis in Ref. [37] which has been found to give good results for low Mach numbers and rather low frequencies [38–40]. An area contraction is formed at the inlet of the cooling tubes. Depending on the flow situation, a vena contracta can be formed just after the area contraction. This implies some dissipation that can be treated using a similar approach as for the expansion [40] but here the isentropic contraction must be added.

3.3.1. Area expansion

The model for the area expansion is derived assuming incompressible mean flow and quasi-steady conditions. As the situation is not isentropic the conservation of momentum over the expansion is used as

$$P_1 S_2 + \rho_0 U_1^2 S_1 = P_2 S_2 + \rho_0 U_2^2 S_2, \tag{92}$$

where P_n is the static pressure, U_n the mean axial flow velocity and the indices 1 and 2 are referring to Fig. 7a. Conservation of mass yields

$$S_1 U_1 = S_2 U_2. \tag{93}$$

Assuming constant density, $\rho_1 = \rho_2 = \rho_0$, and superimposed mean flow the pressure and velocity field can be divided as

$$P_1 = p_{01} + p_1', \quad U_1 = U_{01} + u_1' \tag{94}$$

and

$$P_2 = p_{02} + p_2', \quad U_2 = U_{02} + u_2'. \tag{95}$$

Together with the open area relation $m_{\mathrm{EXP}} = S_1/S_2$, Eq. (92) simplifies to

$$p_1' = p_2' + 2\rho_0 U_{02} u_2' - 2\rho_0 m_{\mathrm{EXP}} U_{01} u_1'. \tag{96}$$

where second-order components have been neglected and the steady components subtracted. The transfer-matrix relation can thereafter be calculated as

$$\begin{bmatrix} p_1' \\ q_1' \end{bmatrix} = \begin{bmatrix} 1 & 2Z_2 M_{02}\left(1 - \dfrac{1}{m_{\mathrm{EXP}}}\right) \\ 0 & 1 \end{bmatrix} \begin{bmatrix} p_2' \\ q_2' \end{bmatrix}, \tag{97}$$

where the wave impedance is $Z_2 = \rho_0 c_0 / S_2$ and the Mach number is $M_{02} = U_{02}/c_0$.

3.3.2. Area contraction

For the case of an area contraction, as shown in Fig. 7b, the flow is homogenous and without losses at the large section (1) and up to the possible vena contracta (c). The vena contracta might exist for situations where

the Reynolds number in the cooling tube is low. The extra losses introduced by the small expansion will be included in the derivation below but will for most cases be very small. Here the conservation of energy is described using Bernoulli's equation for the mean flow between Section 1 and the vena contracta as

$$P_1 + \frac{1}{2}\rho_0 U_1^2 = P_c + \frac{1}{2}\rho_0 U_c^2. \tag{98}$$

Between section (c) and (2) a non-reversible expansion takes place which can be described using the conservation of momentum in Eq. (92). Here the indices have to be changed, which yields

$$P_c S_2 + \rho_0 U_c^2 S_c = P_2 S_2 + \rho_0 U_2^2 S_2. \tag{99}$$

Using Eq. (99) in Eq. (98) together with conservation of mass as stated in Eq. (93) yields

$$p_1' = p_2' + Z_1 M_{01} q_2' \left[\frac{1}{m_{21}^2}\left(\frac{1}{m_{c2}^2} - \frac{2}{m_{c2}} + 2\right) - 1\right], \tag{100}$$

where the area ratios are defined as $m_{21} = S_2/S_1$ and $m_{c2} = S_c/S_2$. For the case without losses Eq. (100) simplifies to

$$p_1' = p_2' + Z_1 M_{01} q_2' \left[\frac{1}{m_{21}^2} - 1\right], \tag{101}$$

Finally the transfer-matrix relation can be calculated as

$$\begin{bmatrix} p_1' \\ q_1' \end{bmatrix} = \begin{bmatrix} 1 & Z_1 M_{01}\left[\frac{1}{m_{21}^2}\left(\frac{1}{m_{c2}^2} - \frac{2}{m_{c2}} + 2\right) - 1\right] \\ 0 & 1 \end{bmatrix} \begin{bmatrix} p_2' \\ q_2' \end{bmatrix}. \tag{102}$$

The ratio that includes the vena contracta area depends on the shape of the inflow and is approximately between 0.5 and 1 [41] with an expected value between 0.61 and 0.65. More accurate estimates can be obtained either by approximate calculations or from experiments.

4. Measurements

In order to validate the proposed model, measurements have been performed using the flow acoustic test facility available at MWL/KTH. All experiments were done at room temperature for different flow speeds. The Mach number in the main ducts was varied between 0 and 0.1 in steps of 0.025, values chosen as being representative for engine operating conditions. This implies that in the cooling tubes, where the area is expanded by a factor 1.2–1.3 compared to the measurement duct, the Mach number will be as most 0.08. The test ducts used during the experiments consisted of standard steel pipes, with diameters equal to 66 mm, chosen in order to relate to the in- and outlet of the charge air coolers. Eight loudspeakers, equally divided between the up- and downstream side of the rig, were used as acoustic sources, as shown in Figs. 8 and 9. The test rig is terminated at each end by a dissipative silencer and a horn to reduce the effects of standing waves.

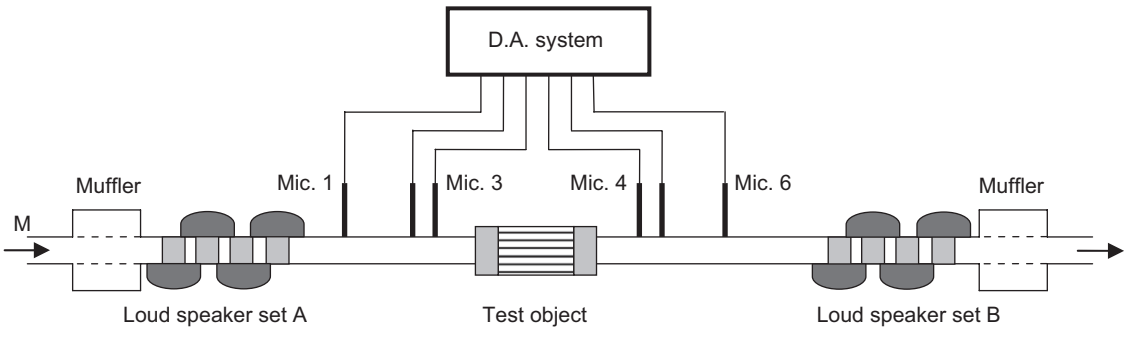

Fig. 8. Layout of the MWL/KTH test rig for determination of acoustic two-port data.

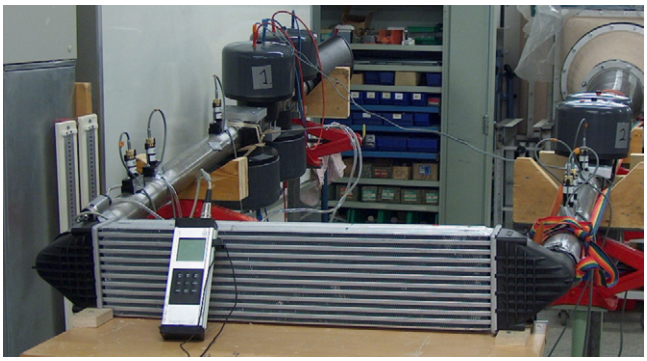

Fig. 9. Photo of the CAC mounted in the MWL/KTH test rig for determination of acoustic two-port data.

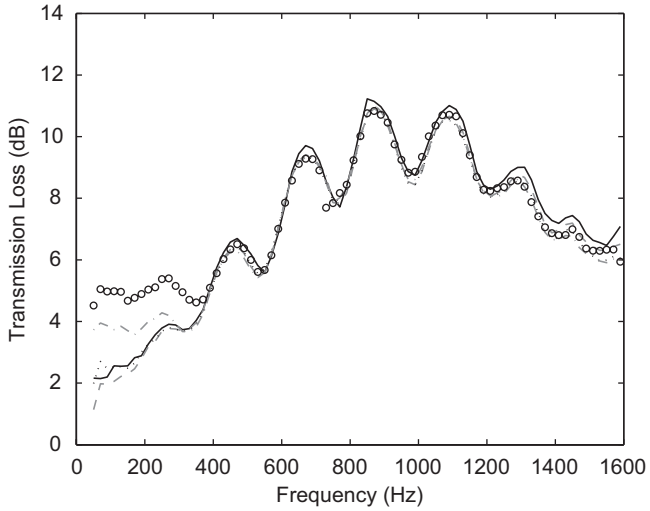

Fig. 10. Measured transmission loss for the complete CAC in the downstream direction: —, $M = 0.0$; - - - -, $M = 0.025$; · · · ·, $M = 0.05$; - · - ·, $M = 0.075$; ◦◦◦◦, $M = 0.01$.

Fluctuating pressures were measured by using six condenser microphones (Brüel & Kjaer 1/4-inch 4938) flush mounted in the wall of the steel pipes. All measurements were performed using random noise excitation. The fluctuating pressures were transformed to the frequency domain with a resolution of 5 Hz and 4000 averages. The two-port matrix for the test object was obtained using the source switching technique as described in Ref. [42]. From the measured two-port data the transmission loss for the CAC was calculated using the expression [23]

$$TL = 10\log\left\{\left(\frac{1+M_{IN}}{1+M_{OUT}}\right)^2\frac{Z_{OUT}}{4Z_{IN}}\left|T_{11}+\frac{T_{12}}{Z_{OUT}}+Z_{IN}T_{21}+\frac{Z_{IN}T_{22}}{Z_{OUT}}\right|^2\right\} \tag{103}$$

and thereafter compared to the transmission loss predicted from theory. The Mach numbers and the acoustic wave impedances in the in- and outlet of the CAC are denoted M_{IN}, M_{OUT}, Z_{IN} and Z_{OUT} in Eq. (103). To minimize the effects of flow noise at the microphones, source correlation using the loudspeaker voltage signal was performed.

The transmission loss obtained from measurements in the direction of flow is shown in Fig. 10. The effect of the mean flow appears to be small at higher frequencies with differences of less than 1 dB. As expected, an increased flow speed will result in decreased damping. An interesting feature is the substantial amount of low

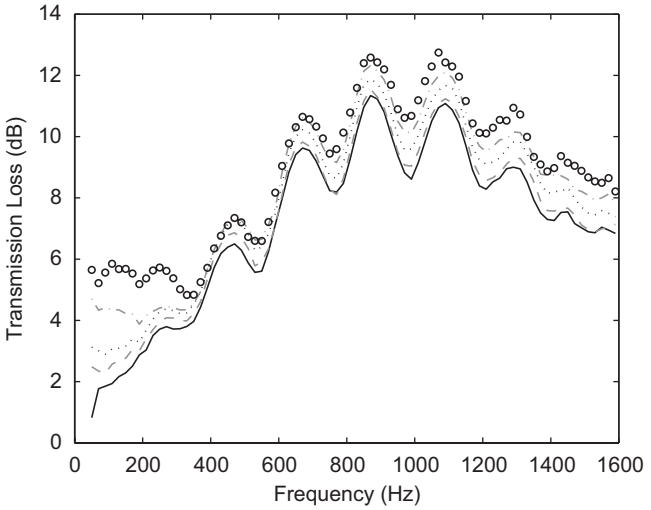

Fig. 11. Measured transmission loss for the complete CAC in the upstream direction: —, $M = 0.0$; - - - -, $M = 0.025$; · · · ·, $M = 0.05$; - · - ·, $M = 0.075$; ◦◦◦◦, $M = 0.01$.

frequency damping that clearly increases with increasing Mach number. As will be seen in the simulation results, this effect can be explained by Howe's theory as transfer of acoustic energy to the turbulent field due to acoustic boundary layers that are thicker than the viscothermal sub-layers. If the engine breathing noise is considered as the source the transmission loss in the upstream direction is more interesting since the CAC is located on the intake side of the engine. The upstream transfer matrix ($\mathbf{T}_{\text{up}}$) can easily be obtained simply by inversion of the downstream transfer matrix ($\mathbf{T}_{\text{down}}$). In order to correctly establish the directions for the velocities, the signs of the elements at the positions (1, 2) and (2, 1) have to be reversed as

$$\mathbf{T}_{\text{up}} = \frac{1}{\mathbf{T}_{\text{down},11}\mathbf{T}_{\text{down},22} - \mathbf{T}_{\text{down},12}\mathbf{T}_{\text{down},21}} \begin{bmatrix} \mathbf{T}_{\text{down},22} & \mathbf{T}_{\text{down},12} \\ \mathbf{T}_{\text{down},21} & \mathbf{T}_{\text{down},11} \end{bmatrix}. \tag{104}$$

Finally, the transmission loss in the upstream direction can be calculated using Eq. (103). The resulting transmission loss is shown in Fig. 11. The effect of the mean flow is more pronounced than in the downstream direction especially at higher frequencies where increasing flow speed corresponds to increasing damping. At low frequencies the damping due to sound-turbulence interaction is about 1 dB larger than in the downstream direction. It is interesting to detect this relatively large amount of turbulent damping for this charge air cooler compared to catalytic converters and particular filters where no effect of turbulence is present.

5. Model validation at cold conditions

5.1. The case without mean flow

5.1.1. Cooling tubes

The effect of using different cross-sectional shapes with identical hydraulic diameter to model the cooling tubes is first studied for the case without flow. Two models are used for this purpose: one 1D axi-symmetric circular model and one 2D model with the shape of an isosceles trapezium—in this particular case very similar to a triangle. The 2D mesh, which is shown in Fig. 12, is symmetric in one direction and is therefore represented by half the geometry. The axi-symmetric mesh, which is biased towards the duct wall in order to resolve the large gradients in the boundary layers, consists of 19 elements and 39 nodes. Corresponding figures for the 2D trapezium geometry are 270 elements and 1155 nodes. The calculated attenuation and phase speed ratio for the two models are shown in Figs. 13 and 14. Here, the attenuation and phase speed ratio of a wave

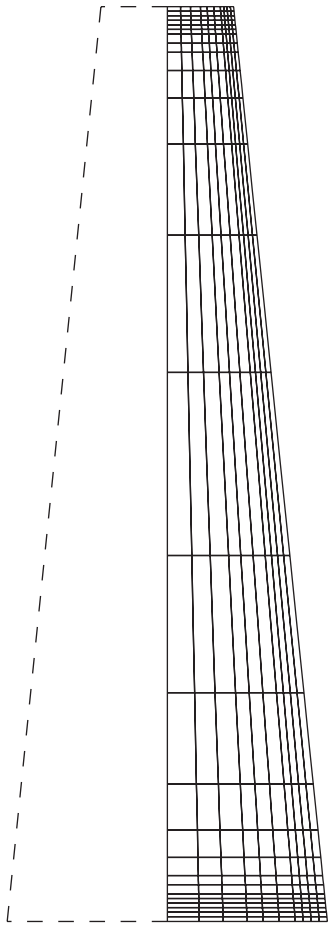

Fig. 12. 2D finite element mesh used to describe the two-ports for the cooling tubes.

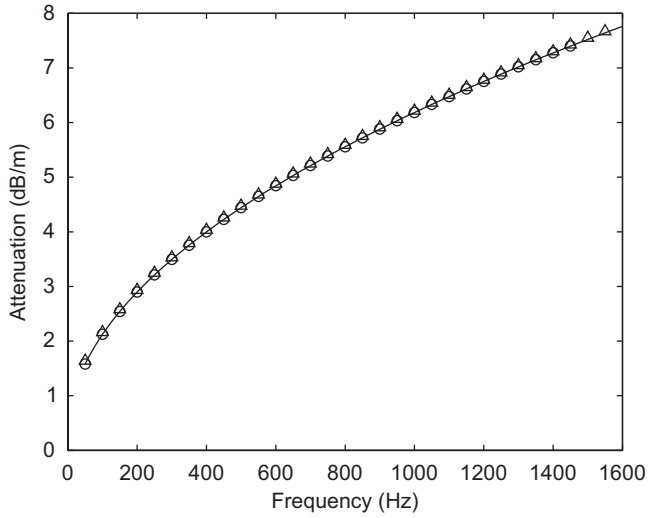

Fig. 13. Predicted attenuation for one cooling tube: —, Zwikker & Kosten; ○○○○, 2D FE: circular geometry; ΔΔΔΔ, 2D FE: trapezium geometry.

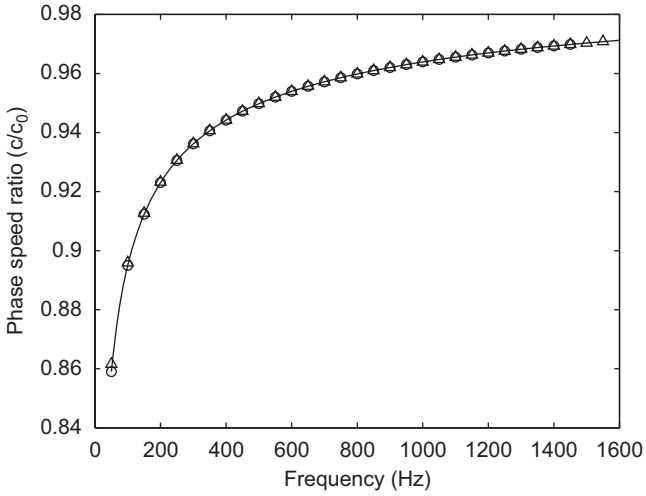

Fig. 14. Predicted phase speed ratio for one cooling tube: —, Zwikker & Kosten; ○○○○, 2D FE: circular geometry; ΔΔΔΔ, 2D FE: trapezium geometry.

are defined as

$$\text{attenuation} = 8.686|\text{Im}(k_0\Gamma)| \quad (\text{dB/m}) \tag{105}$$

and

$$c/c_0 = |1/\text{Re}(\Gamma)|. \tag{106}$$

The difference between the Zwikker and Kosten solution and the one obtained from using the 1D FE solution for a circular cross-section is less than $0.01\,\text{dB}\,\text{m}^{-1}$, which indicates that the element discretization has converged. In Fig. 13 it can also be noticed that the difference between the circular solution and the trapezium solution is very small and decreases with increasing frequency. There is less than $0.1\,\text{dB}\,\text{m}^{-1}$ more damping for the trapezium solution. The trend is similar for the phase speed ratio (see Fig. 14).

If the hydraulic diameter is used to calculate the shear wavenumber, the lower frequency limit at 50 Hz will correspond to a shear wavenumber of $s = 6$ whereas the upper frequency limit at 1600 Hz corresponds to $s = 35$. The "reduced frequency" for the frequency extremes are $k_0a = 0.0012$ and 0.040, respectively. The requirements that $k_0a \ll 1$ and $k_0a/s \ll 1$ are thereby fulfilled and the Zwikker and Kosten approximations are valid [13]. The lower shear wavenumber is definitely in the same range as the catalytic converters that were studied in Refs. [14,15]. The upper limit, however, far exceeds the shear wavenumber of 10 that was the largest reported. This indicates that the wide duct approximation by Kirchhoff might also be a good choice to simplify the calculations. The axial velocity profile, which was observed in Ref. [13] to consist of an almost flat core and small peaks close to the tube wall, is also present for the trapezium geometry (see Fig. 15), which emphasizes the need of a biased mesh with fine resolution close to the walls.

5.1.2. Complete charge air cooler

The complete charge air cooler is modelled using two approaches: completely based on two-ports using the SIDLAB software [43] or based on the multi-port approach to represent the tanks together with two-ports for the cooling tubes as was described in Section 3. In order to study the sensitivity to the amount of damping in the 3D FE-models used to obtain the multi-ports, two different values on the speed of sound are used: $c = c_0$ and $c = c_0(1 + i/100)$ where c_0 is the isentropic speed of sound and i is the imaginary number. This artificial damping will compensate the FE-results for the viscothermal losses occurring at the boundaries, damping in the plastic walls and radiation. The chosen damping value is based on measurements and modelling done on similar plastic components in Ref. [35], see also Section 3.2.1.

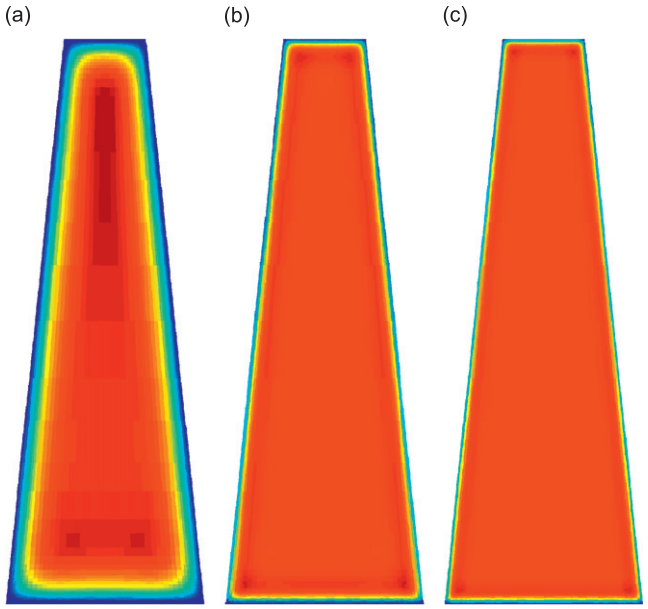

Fig. 15. Predicted normalized acoustic velocity mode shapes for (a) 50 Hz; (b) 500 Hz and (c) 1000 Hz.

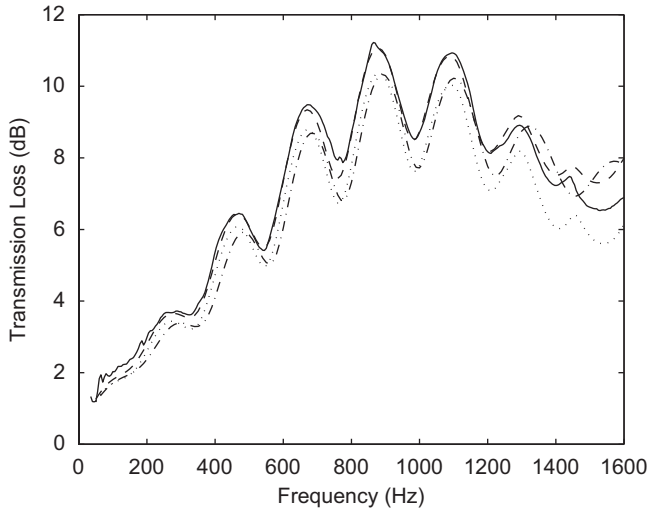

Fig. 16. Transmission loss for complete CAC at $M = 0$: —, measured; - - - -, predicted using multi-port technique and 2D FE trapezium geometry (speed of sound $c = c_0(1 + i/100)$ in 3D FE-model); · · · ·, predicted using multi-port technique and 2D FE trapezium geometry (speed of sound $c = c_0$ in 3D FE-model); - · - · , predicted using two-port technique and 2D FE trapezium geometry.

In Fig. 16 the transmission loss from these three predictions is shown together with the experimentally obtained curve. It can be observed that the two-port approach provides good results with deviations less than 1 dB up to 1200 Hz where cross-modes in the inlet/outlet tanks start to propagate and the response is shifted. The accuracy of the results provided from the multi-port approach with complex speed of sound is very good. The deviation stays within less than 0.5 dB up to 1400 Hz, indeed an impressive result. Above 1400 Hz the deviation is between 0.5 and 1 dB which still is a good result. The predictions made without losses in the tanks, are not as good with deviations increasing with increasing frequency. In the following calculations, for the case of superimposed flow, the speed of sound $c = c_0(1 + i/100)$ is used in the 3D FE-model used to extract the multi-ports.

5.2. The case with mean flow

5.2.1. Cooling tubes

The study of the dependence on using circular or trapezium shape to model the cooling tubes is extended here to include a small mean flow. The effect of approximating the profile of the mean flow as constant compared to a laminar profile is also studied. For this purpose the model by Dokumaci [14] and the modified 2D FE approach [16] is used. The flow speed in the tubes was taken as $M = 0.08$ which corresponds to $M = 0.1$ in the measurement ducts (diameter 0.066 m). If the hydraulic diameter is used the Reynolds number becomes $Re = 5000$, which for a circular cross-section indicates that the flow is not laminar but rather turbulent or in the transition zone. For triangular sections, as was discussed in Section 2, transition occurs

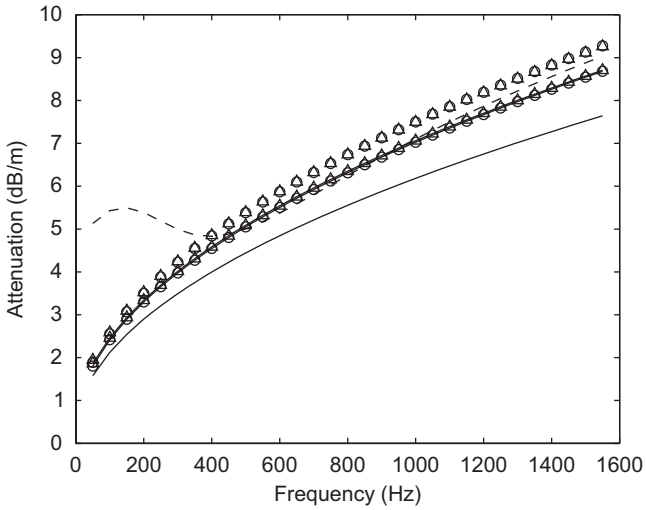

Fig. 17. Predicted attenuation in the upstream direction for one cooling tube at $M = 0.08$: —, Zwikker & Kosten ($M = 0$); ⊖⊖⊖⊖, Dokumaci (flat mean flow profile); ΔΔΔΔ, 2D FE: trapezium geometry (flat mean flow profile); ○○○○, 2D FE: circular geometry (laminar mean flow profile); ΔΔΔΔ, 2D FE: trapezium geometry (laminar mean flow profile), - - - - Howe.

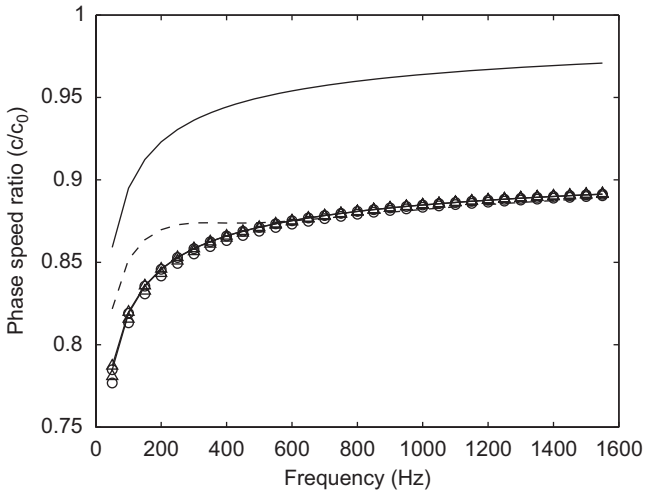

Fig. 18. Predicted phase speed ratio in the upstream direction for one cooling tube at $M = 0.08$: —, Zwikker & Kosten ($M = 0$); ⊖⊖⊖⊖, Dokumaci (flat mean flow profile); ΔΔΔΔ, 2D FE: trapezium geometry (flat mean flow profile); ○○○○, 2D FE: circular geometry (laminar mean flow profile); ΔΔΔΔ, 2D FE: trapezium geometry (laminar mean flow profile), - - - - Howe.

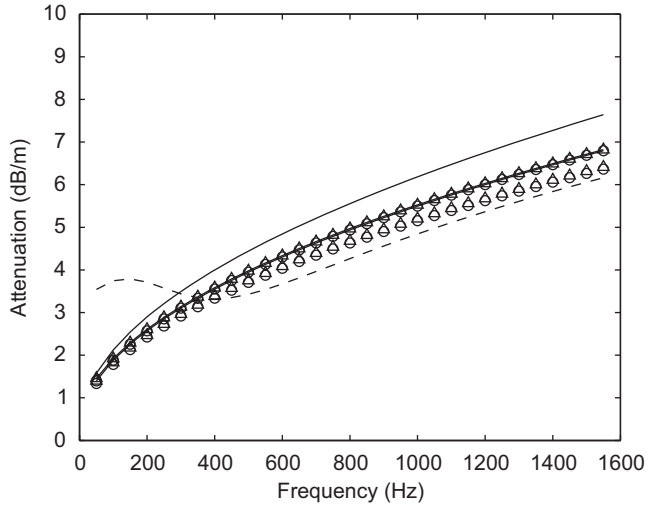

Fig. 19. Predicted attenuation in the downstream direction for one cooling tube at $M = 0.08$: —, Zwikker & Kosten ($M = 0$); ⊖⊖⊖⊖, Dokumaci (flat mean flow profile); ΔΔΔΔ, 2D FE: trapezium geometry (flat mean flow profile); ○○○○, 2D FE: circular geometry (laminar mean flow profile); ΔΔΔΔ, 2D FE: trapezium geometry (laminar mean flow profile), ---- Howe.

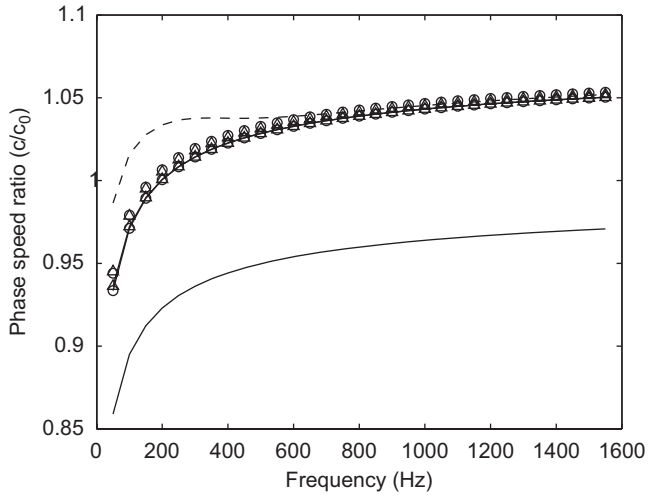

Fig. 20. Predicted phase speed ratio in the downstream direction for one cooling tube at $M = 0.08$: —, Zwikker & Kosten ($M = 0$); ⊖⊖⊖⊖, Dokumaci (flat mean flow profile); ΔΔΔΔ, 2D FE: trapezium geometry (flat mean flow profile); ○○○○, 2D FE: circular geometry (laminar mean flow profile); ΔΔΔΔ, 2D FE: trapezium geometry (laminar mean flow profile), ---- Howe.

gradually over the cross-section when the Reynolds number is increased. It is therefore not possible to state whether the flow is laminar or turbulent in the entire cross-section for this flow speed. In order to find out if the low frequency damping that was observed in the experiments for this flow speed is related to interaction between the acoustic boundary layers and the turbulence, the model by Howe is used. To the authors' knowledge, no data has been published using this model for Reynolds numbers below $Re = 10\,000$. The model requires that the mean flow profile is flat which might not be the case for the less turbulent flow in this particular case.

Figs. 17 and 18 show the attenuation and phase speed ratio in the direction opposite to the mean flow for the predictions. The difference between using the trapezium geometry and the circular one is very small for both the case of constant and laminar flow profile. The difference relative to the laminar flow solution is in the order of 1% and decreases with increasing frequency. Moreover, it is interesting that the plug flow profile

solution underestimates the damping compared to the corresponding laminar flow profile solution. The difference, which is of the order of 6% relative to the laminar flow solution, increases with increasing frequency. Concerning the phase speed ratio the relative differences are even smaller and are all decreasing with increasing frequency. Identical observations can also be made for waves propagating with the mean flow, see Figs. 19 and 20. However, here the damping is less than for the case without flow and the laminar flow profile solution gives even less damping than the plug flow solution.

The effect of excluding the fluctuating part of the dissipation function is not included in the figures as it is extremely small for this particular case. For the circular cross-section, where the laminar flow profile can be obtained from the Hagen-Poiseuille solution, the relative error from neglecting the dissipation term is less than 0.5% at a Stokes number of 6 (50 Hz) and decreases with increasing frequency. For very low frequencies the effect can be significant as the error increases steeply with decreasing frequency, however, in the frequency range of interest in the present investigation the simplification is justified.

The solution obtained using the model by Howe captures the effect of low frequency damping in both directions as expected. However, the high frequency behaviour is based on the truncated "wide" Kirchhoff solution in Ref. [13] and therefore results in less damping than the Zwikker &; Kosten solution in the low flow limit.

5.2.2. Complete charge air cooler

For the case of a complete CAC and a present mean flow the multi-port approach is used to represent the tanks together with two-ports for the cooling tubes. To represent the cooling tubes it was decided to use the two-ports obtained in the previous section from the 2D FE model (trapezium geometry) with laminar mean flow profile and the model by Howe ($M = 0.08$). The models assuming a flat mean flow profile will produce results somewhere in between these two. The profile of the actual mean flow is not known, as was discussed in Section 2.1, and will also change along the axial direction since the zone of unestablished flow might be of significant length.

The coupling elements for cross-sectional area discontinuities that were described in Section 3.3 are used with an open area ratio of 0.61 for the vena contracta appearing at the inlet to the cooling tubes. This approximate value can probably be improved but will most likely be larger, which is why this estimate is conservative [41]. The effect on the assembled CAC is, however, very small. The predicted and measured transmission loss for sound propagating through the CAC in the upstream direction is shown in Fig. 21. The high frequency estimate from using 2D FE shows very good agreement with the experimentally obtained

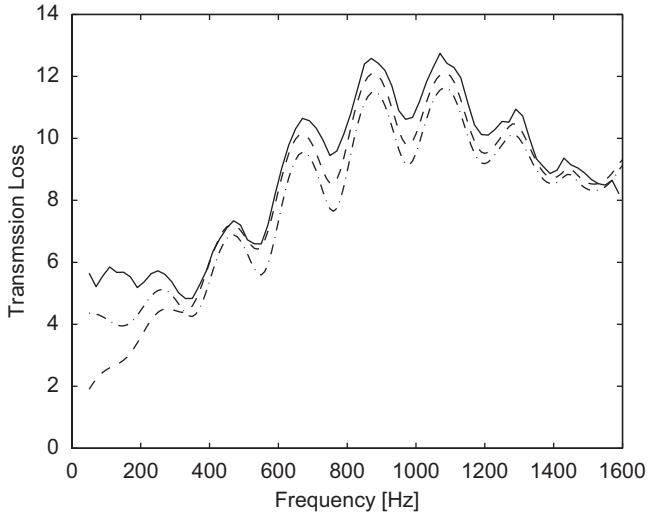

Fig. 21. Transmission loss in the upstream direction for complete CAC at $M = 0.1$ in main duct ($M = 0.08$ in cooling tubes): —, measured; - - - -, predicted using multi-port technique and 2D FE (trapezium geometry) with laminar mean flow profile; - · - · -, predicted using multi-port technique and Howe's model.

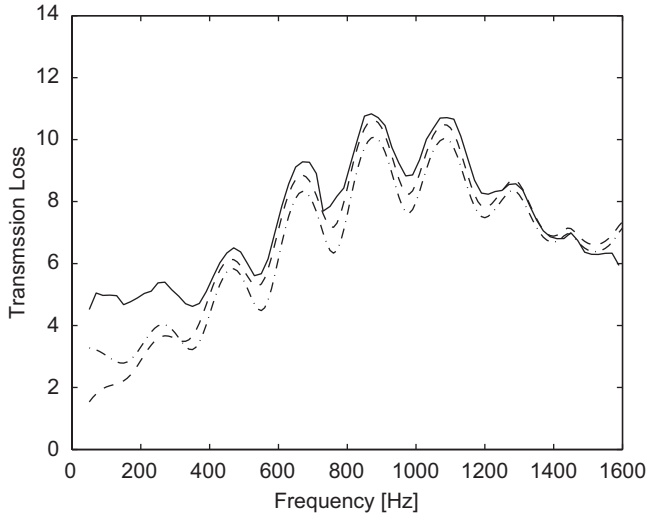

Fig. 22. Transmission loss in the downstream direction for complete CAC at $M = 0.1$ in main duct ($M = 0.08$ in cooling tubes): —, measured; - - - -, predicted using multi-port technique and 2D FE (trapezium geometry) with laminar mean flow profile; - · - · -, predicted using multi-port technique and Howe's model.

except in the frequency band between 700 and 1000 Hz where some minor discrepancies can be observed. Possible explanations for those deviations might be the effect of neglecting the dissipation that is included in the original derivation in Ref. [16], from neglecting the matching of the near fields when coupling the two-ports to the tanks or from neglecting the in-plane velocity components that was shown in Ref. [19] to yield increasing effects when the shear wavenumber is increased.

Although the model by Howe does not yield as good predictions as the 2D FE solution in the high frequency band, where the deviation is about 1 dB, it gives the best estimates in the low frequency band up to 300 Hz. The model does still give an under-prediction of the measurement data but the effect of extra damping, due to the interaction between the turbulence and the sound field, is captured, which cannot be achieved by the 2D FE solution.

Similar observations can be made for the case where the two-port is in the same direction as the mean flow (see Fig. 22). The predicted attenuation is smaller than that obtained experimentally. The deviation in the high frequency domain is slightly larger for the 2D FE solution than in the upstream direction but stays within 1 dB while the model by Howe shows the same accuracy as before. The low frequency prediction is, however, slightly worsened and gives an underestimate of approximately 2 dB. For low frequencies when the wave length is much smaller than the length scale of the CAC, the transmission will be defined by the pressure drop. The transmission loss should therefore be independent of the direction of the two-port, which is almost the case in the measurements. Why the results from using Howe's model do not show this behaviour is not completely understood. One possible explanation could be that Howe's model assumes that the sub-layers are thin which might not be the case for the Reynolds number appearing in this study.

6. Predicted damping for a CAC at operating conditions

To investigate the acoustical properties for a CAC at operating conditions the gas properties are updated to correspond to values taken upstream and downstream of a CAC mounted on an operating engine. This engine is a five cylinder diesel engine and the values in Table 1 were taken in an engine test bench at an engine revolution speed of 4200 rev/min where the mass flow was 663 kg h^{-1}.

The density is calculated using the law of ideal gases, the dynamic viscosity, the thermal conductivity and the specific heat capacity at constant pressure are only dependent on the temperature at these low pressures and can be taken from standard books [44]. The isentropic speed of sound is calculated as $c_0 = \sqrt{\gamma RT}$.

Table 1
Gas data at operating conditions for five cylinder diesel engine

	Upstream CAC	Downstream CAC
Temperature (K)	443	340
Static pressure (kPa)	253	244
Reynolds number (—)	4900	5900
Mach number (—)	0.052	0.047
Speed of sound ($m\,s^{-1}$)	442	370
Density ($kg\,m^{-3}$)	1.99	2.50
Dynamic viscosity $\times 10^5$ (Pa s)	2.44	2.01

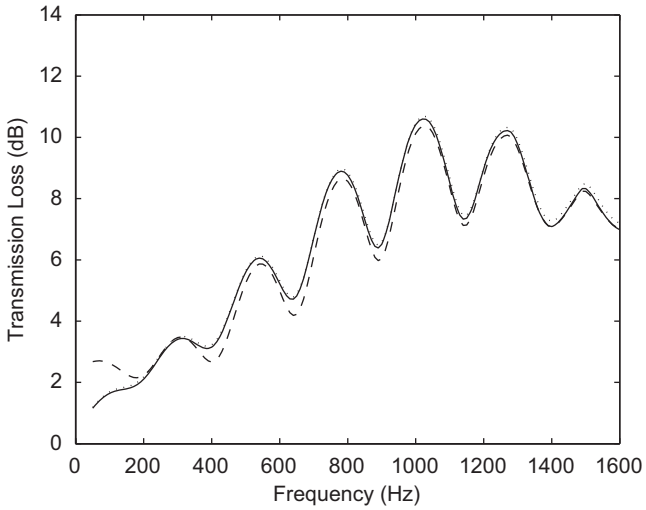

Fig. 23. Transmission loss in the upstream direction versus frequency for CAC mounted on engine operating at 4200 rev/min: —, predicted using multi-port technique and Dokumaci's model [14]; ---- predicted using multi-port technique and Howe's model [26], · · · · predicted using multi-port technique and 2D FE with circular geometry and laminar mean flow.

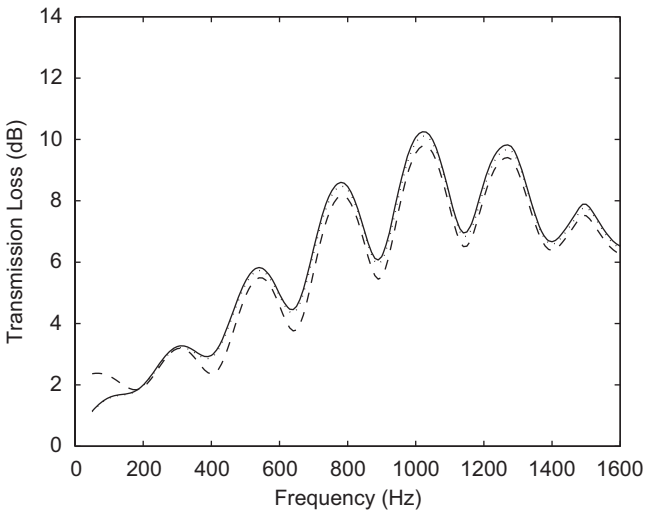

Fig. 24. Transmission loss in the downstream direction versus frequency for CAC mounted on engine operating at 4200 rev/min: —, predicted using multi-port technique and Dokumaci's model [14]; ---- Predicted using multi-port technique and Howe's model [26], · · · · predicted using multi-port technique and 2D FE with circular geometry and laminar mean flow.

Three different solutions are used to extract the two-ports that are used together with the multi-port approach. The geometry is approximated as circular and the shape of the incompressible mean flow profile is regarded as flat or laminar. Laminar as well as turbulent flow are considered. The temperature and pressure gradient can be treated by dividing the cooling tubes into several two-ports based on different gas properties coupled in cascade as was shown in Refs. [27,38]. The convergence is, however very fast and the difference between using one two-port and ten results in differences less than 0.1 dB. The predicted transmission loss in the upstream direction for the complete CAC at operating conditions is shown in Fig. 23. The gas properties in the tanks are based on the up- and downstream values from Table 1 and the two-ports representing the cooling tubes are calculated using the average values.

The difference between the three solutions is very small and stays within 0.5 dB except in the low frequency region where the model by Howe yields about 2 more dB as expected. The transmission loss is generally smaller than for the cold case and the distance between the peaks are larger due to the larger speed of sound at higher temperatures. The low frequency damping is just between 2 and 3 dB which is smaller than the 4–5 dB that was predicted at cold conditions. Bearing in mind the difference between predictions and measurements at cold conditions, there is probably one extra dB not predicted that can be added for the hot case as well, thus resulting in 3–4 dB. Concerning transmission loss in the direction of flow, the conclusions are similar (see Fig. 24). The difference between the two directions is less than 1 dB in the range between 50 and 1600 Hz.

7. Summary and conclusions

Sound transmission through charge air coolers has been studied. The frequency range under consideration was low and medium where non-plane waves exist in the inlet/outlet tanks. A new hybrid methodology for calculation of the global acoustic two-port for an automotive intake/exhaust device consisting of volumes with multiple openings coupled to narrow channels has been proposed. An attractive formalism for extraction of multi-ports from numerical 3D finite elements has been derived and presented. The two-ports for the narrow channels include a complete treatment of the losses due to viscous and thermal boundary layers for cases without flow as well as with a superimposed mean flow. The 2D finite element scheme derived by Astley and Cummings [16] and the model by Dokumaci [14] have been used to study the effect of using an isosceles trapezium or a circular cross-section with equivalent hydraulic diameter for the narrow channels. The effect of the shape of the cross-section has been found to be small, but increases with increasing mean flow. Flat profiles as well as laminar flow profiles have been used for the superimposed incompressible mean flow and the difference between these has been shown to be of larger importance than the shape of the cross-section.

The hybrid methodology has been applied as the first complete model for charge air coolers. The model has been validated to experimentally obtained transmission loss data at room temperature for a charge air cooler designed for use on a passenger car with very good accuracy. For the case of a superimposed mean flow, a considerable amount of low frequency damping due to turbulence has been observed. The model for interaction between sound waves and turbulence proposed by Howe [26] has for the first time been applied to extract two-ports. The use of these two-ports within the hybrid model describes the low frequency attenuation with reasonable accuracy but gives slightly less accurate predictions at higher frequencies.

The proposed models have been used to predict the sound transmission through the charge air cooler at operating conditions. Mass flow, temperature and pressure data for the enclosed air, taken at positions upstream and downstream of a CAC mounted on an engine in test bench, was used to calculate the required gas properties. The predicted transmission loss at operating conditions is smaller than those obtained at cold conditions without pressure and temperature gradients. The amount of damping is, however, still significant at all frequencies which gives previously underestimated opportunities to control the final noise spectra of turbocharged engines.

Acknowledgements

The work described in this paper was funded by Volvo Car Corporation, EMFO—the Swedish Emission Research Programme and KTH CICERO—Centre for Internal Combustion Engine Research Opus. This funding is gratefully acknowledged by the authors.

References

[1] T. Raitor, W. Neise, Sound generation in centrifugal compressors, *Proceedings of the 12th AIAA/CEAS Aero Acoustic Conference*, Cambridge, MA, USA, 2006, pp. 1–26.

[2] H. Rämmal, M. Åbom, Acoustics of turbochargers, SAE Technical Paper 2007-01-2205, 2007.

[3] J.M. Desantes, A.J. Torregrosa, A. Broatch, H. Climent, Silencing capabilities of non-silencer elements: an underused potential? *Proceedings of the Fourth Styrian Noise, Vibration and Harshness Congress*, Graz, Austria, 2006, pp. 105–122.

[4] H. Rafael, *A two-port model for a turbo charger compressor and intercooler*, M.Sc. Thesis, Royal Institute of Technology, Stockholm, Sweden, 2000.

[5] D. Jung, D. Assanis, Numerical modelling of cross flow compact heat exchanger with louvered fins using thermal resistance concept, SAE Technical Paper 2006-01-0726, 2006.

[6] K. Nakonieczny, Numerical modelling of cross-flow plate-fin air-to-air heat exchanger under unsteady flow conditions, *Numerical Heat Transfer Part A—Applications* 49 (1) (2006) 1–24.

[7] P.A. Bromnick, R.J. Pearson, D.E. Winterbone, Intercooler model for unsteady flows in engine manifolds, *Journal of Automotive Engineering* 212 (1998) 119–132.

[8] J. Galindo, J.R. Serrano, H. Climent, F.J. Arnau, New one-dimensional fluid-dynamic model for automotive intercoolers, *Proceedings of EAEC Eighth European Automotive Congress*, Bratislava, Slovakia, 2001, pp. 1–9.

[9] M. Knutsson, M. Åbom, Acoustic analysis of charge air coolers, SAE Technical Paper 2007-01-2208, 2007.

[10] M. Knutsson, M. Åbom, Sound propagation in narrow channels with arbitrary cross sections and superimposed mean flow with application to charge air coolers, *Proceedings of the 14th International Congress on Sound and Vibration*, Cairns, Australia, 2007.

[11] G. Kirchhoff, Uber den einfluss der wärmteleitung in einem gas auf die schallbewegung, *Annalen der Physik und Chemie* 134 (6) (1868) 177–193.

[12] C. Zwikker, C.W. Kosten, *Sound Absorbing Materials*, Elsevier, Amsterdam, 1949.

[13] H. Tijdeman, On the propagation of sound waves in cylindrical tubes, *Journal of Sound and Vibration* 39 (1) (1975) 1–33.

[14] E. Dokumaci, Sound transmission in narrow pipes with superimposed uniform mean flow and acoustic modelling of automobile catalytic converters, *Journal of Sound and Vibration* 182 (5) (1995) 799–808.

[15] E. Dokumaci, On transmission of sound in circular and rectangular narrow pipes with superimposed mean flow, *Journal of Sound and Vibration* 210 (3) (1998) 375–389.

[16] R.J. Astley, A. Cummings, Wave propagation in catalytic converters: formulation of the problem and finite element scheme, *Journal of Sound and Vibration* 188 (5) (1995) 635–657.

[17] K.S. Peat, A first approximation of the effects of mean flow on sound propagation in capillary tubes, *Journal of Sound and Vibration* 175 (4) (1994) 475–489.

[18] J.-G. Ih, C.M. Park, H.J. Kim, A model for sound propagation in capillary ducts with mean flow, *Journal of Sound and Vibration* 190 (2) (1996) 163–175.

[19] K.W. Jeong, J.-G. Ih, A numerical study on the propagation of sound through capillary tubes with mean flow, *Journal of Sound and Vibration* 198 (1) (1996) 67–79.

[20] K.S. Peat, Convected acoustic wave motion along a capillary duct with an axial temperature gradient, *Journal of Sound and Vibration* 203 (5) (1997) 855–866.

[21] K.S. Peat, R. Kirby, Acoustic wave motion along a narrow cylindrical duct in the presence of an axial mean flow and temperature gradient, *Journal of the Acoustical Society of America* 107 (4) (2000) 1859–1867.

[22] E. Dokumaci, An approximate dispersion equation for sound waves in a narrow pipe with ambient gradients, *Journal of Sound and Vibration* 240 (4) (2001) 637–646.

[23] M.L. Munjal, *Acoustics of Ducts and Mufflers*, Wiley, New York, 1987.

[24] H. Schlichting, *Boundary Layer Theory*, McGraw-Hill, New York, 1979.

[25] E.R.G. Eckert, T.E. Irvine, Flow in corners of passages with noncircular cross sections, *Transactions of the American Society of Mechanical Engineers* 78 (1956) 709–718.

[26] M.S. Howe, The damping of sound by wall turbulent shear layers, *Journal of the Acoustical Society of America* 98 (3) (1995) 1723–1730.

[27] S. Allam, M. Åbom, Modelling and testing of after-treatment devices, *Journal of Vibration and Acoustics* 128 (2006) 347–356.

[28] D. Ronneberger, C.D. Ahrens, Wall shear stress caused by small amplitude perturbations of turbulent boundary-layer flow: an experimental investigation, *Journal of Fluid Mechanics* 83 (4) (1977) 433–464.

[29] M.C.A.M. Peters, A. Hirschberg, A.J. Reijnen, A.P.J. Wijnands, Damping and reflection coefficient measurements at low Mach and low Helmholtz numbers, *Journal of Fluid Mechanics* 265 (1993) 499–534.

[30] U. Ingard, V.K. Singhal, Sound attenuation in turbulent pipe flow, *Journal of the Acoustical Society of America* 55 (1974) 535–538.

[31] S. Allam, M. Åbom, Investigation of damping and radiation using full plane wave decomposition in ducts, *Journal of Sound and Vibration* 292 (2006) 519–534.

[32] M. Åbom, An analytical model for reactive silencers based on Bragg-scattering, *Journal of Sound and Vibration* 112 (2) (1987) 384–388.

[33] O.C. Zienkiewicz, R.L. Taylor, *The Finite Element Method*, fourth ed., McGraw-Hill, New York, 1990.

[34] SYSNOISE rev. 5.6 User's Manual, LMS-Numerical Technologies, Leuven, Belgium, 2005.

[35] M. Knutsson, J. Lennblad, H. Bodén, Prediction of IC-engine intake orifice noise using 3D acoustic modelling and linear source data based on non-linear CFD, *Proceedings of the Fifth Styrian Noise, Vibration and Harshness Congress*, Graz, Austria, 2008.

[36] S. Boij, B. Nilsson, Scattering and absorption of sound at flow duct expansions, *Journal of Sound and Vibration* 289 (3) (2006) 577–594.
[37] R.J. Alfredson, P.O.A.L. Davies, Performance of exhaust silencer components, *Journal of Sound and Vibration* 15 (2) (1971) 175–196.
[38] R. Glav, *On Acoustic Modelling of Silencers*, PhD Thesis, Royal Institute of Technology, Stockholm, Sweden, 1994.
[39] S. Allam, M. Åbom, Sound propagation in an array of narrow porous channels with application to diesel particulate filters, *Journal of Sound and Vibration* 291 (2006) 882–901.
[40] J.-G. Ih, W.-Y. Choi, Sound propagation through the diesel particulate filter, *Proceedings of the 12th International Congress on Sound and Vibration,* Lisbon, Portugal, 2005.
[41] G.K. Batchelor, *An Introduction to Fluid Dynamics*, Cambridge University Press, New York, 2006.
[42] M. Åbom, Measurement of the scattering-matrix of acoustical two-ports, *Mechanical Systems and Signal Processing* 5 (2) (1991) 89–104.
[43] T. Elnady, M. Åbom, SIDLAB: New 1D sound propagation software for complex duct networks, *Proceedings of the 13th International Congress on Sound and Vibration*, Vienna, Austria, 2006.
[44] R.B. Bird, *Transport Phenomena*, Wiley, New York, 1960.